ESAIM: M2AN 50 (2016) 1887–1916
DOI: 10.1051/m2an/2016010

ESAIM: Mathematical Modelling and Numerical Analysis
www.esaim-m2an.org

NONDIFFUSIVE CONSERVATIVE SCHEMES BASED ON APPROXIMATE RIEMANN SOLVERS FOR LAGRANGIAN GAS DYNAMICS

Nina Aguillon[1] and Christophe Chalons[2]

Abstract. In this paper, we present a conservative finite volume scheme for the gas dynamics in Lagrangian coordinates, which is fast and nondiffusive. By fast, we mean that it relies on an approximate Riemann solver, and hence the costly resolution of Riemann problems is avoided. By nondiffusive, we mean that the solution provided by the scheme is exact when the initial data is an isolated admissible shock, and discontinuities are sharply captured in general. The construction of the scheme uses two main tools: the approximate Riemann solver of [Ch. Chalons and F. Coquel, *Math. Models Methods Appl. Sci.* **24** (2014) 937–971.], which turns out to be exact on isolated admissible shocks, and a discontinuous reconstruction strategy, which consists in rebuilding entropy satisfying shocks inside some well chosen cells. Numerical experiments in 1D and 2D are proposed.

Mathematics Subject Classification. 35L65, 35L40, 65M08, 76N15, 76M12.

Received November 10, 2014. Revised October 23, 2015. Accepted January 25, 2016.

1. Introduction

In this paper, we consider the barotropic gas dynamics equations in Lagrangian coordinates

$$\begin{cases} \partial_t \tau - \partial_x u = 0, \\ \partial_t u + \partial_x p(\tau) = 0, \\ \tau(0,x) = \tau^0(x), \ u(0,x) = u^0(x), \end{cases} \tag{1.1}$$

where the pressure law p is a strictly convex and strictly decreasing function. This system is well-known to be strictly hyperbolic, with eigenvalues $\pm\sqrt{-p'(\tau)}$ and two genuinely nonlinear characteristic fields. The phase space Ω of this system is

$$\Omega = \{(\tau, u) \in \mathbb{R}^2, \tau > 0\}.$$

As usual, we supplement (1.1) with the validity of the so-called entropy inequality

$$\partial_t \mathcal{U}(\tau, u) + \partial_x \mathcal{W}(\tau, u) \leq 0, \tag{1.2}$$

Keywords and phrases. Conservative finite volume scheme, discontinuous reconstruction, approximate Riemann solver, non diffusive scheme, Sharp discontinuities.

[1] Sorbonne Universités, UPMC University Paris 06, CNRS, UMR 7598, Laboratoire Jacques-Louis Lions, 4 place 75005 Jussieu, Paris, France. nina.aguillon@upmc.fr

[2] Laboratoire de Mathématiques de Versailles, UVSQ, CNRS, Université Paris-Saclay, 78035 Versailles, France. christophe.chalons@uvsq.fr

Article published by EDP Sciences

© EDP Sciences, SMAI 2016

where $(\mathcal{U}, \mathcal{W})$ is the entropy-entropy flux pair given by

$$\mathcal{U}(\tau, u) = \frac{u^2}{2} + e(\tau), \text{ with } e(\tau) = -\int^{\tau} p(y)dy \text{ and } \mathcal{W}(\tau, u) = p(\tau)u,$$

and we consider entropy weak solutions of (1.1) and (1.2), see [17] for example.

In order to motivate our study, let us temporarily assume that the initial data is a Riemann initial data

$$\begin{cases} \tau^0(x) = \tau_L \mathbf{1}_{x<0} + \tau_R \mathbf{1}_{x>0}, \\ u^0(x) = u_L \mathbf{1}_{x<0} + u_R \mathbf{1}_{x>0}, \end{cases} \tag{1.3}$$

where the left and right states (τ_L, u_L) and (τ_R, u_R) verify the Rankine–Hugoniot relations

$$u_L - u_R = -s(\tau_L - \tau_R) \quad \text{and} \quad p(\tau_L) - p(\tau_R) = s(u_L - u_R), \tag{1.4}$$

for a given speed of propagation s, and the triple $\big((\tau_L, u_L), (\tau_R, u_R), s\big)$ satisfies (1.2) in the weak sense, *i.e.*

$$-s\left(\mathcal{U}(\tau_R, u_R) - \mathcal{U}(\tau_L, u_L)\right) + \left(\mathcal{W}(\tau_R, u_R) - \mathcal{W}(\tau_L, u_L)\right) \leq 0.$$

In that case the initial condition is such that the initial discontinuity will move at velocity s to form an admissible entropy weak solution of (1.1) and (1.2), see again [17]. We say that we have an isolated shock wave.

On the other hand and from the numerical point of view, the Godunov method [18] and Godunov-type methods based on exact or approximate Riemann solvers (see [26] for a review) are certainly the most celebrated numerical schemes that provide good numerical approximations of (1.1) and (1.2) for general initial data. In particular, the Lax–Wendroff theorem (see [17]) ensures the convergence to the entropy weak solution of (1.1) and (1.2) provided that the method does converge and verifies a discrete version of (1.2).

When applied to the particular initial data leading to an isolated shock wave, such conservative finite volume schemes are well-known to introduce numerical diffusion, which means here intermediate values that do not correspond to values taken by the exact solution.

The basic motivation of this work is to propose a new conservative finite volume scheme which will be able to exactly capture isolated shock waves; and more generally entropy weak solutions of (1.1) and (1.2) with no numerical diffusion near shocks. By no numerical diffusion, we mean here that only one intermediate value will be present in shock profiles and importantly that this intermediate value will correspond to the average of the exact solution on a given cell for isolated shock wave. This is of course the best one can do.

To achieve this goal, let us first emphasize that the drawbacks of Godunov and Godunov-type methods are two fold.

- First, the numerical diffusion already discussed above leads to a loss of accuracy of the approximate solutions, especially around discontinuities.
- Second, the Godunov method uses the knowledge of the exact solution of (1.1)−(1.3) with any given left and right states (τ_L, u_L) and (τ_R, u_R) in the phase space Ω. This exact Riemann solver is of course exact when (1.3) is an isolated shock, but it can be very expensive or difficult to compute the exact solution in general. When approximate Riemann solvers are used, it can be much less expensive but the property of being exact when (1.3) is an isolated shock is generally lost.

To avoid these issues, we follow the following strategy. Concerning the first point, *i.e.* removing the numerical diffusion, we use a discontinuous reconstruction strategy. The basic idea is to reconstruct entropy satisfying shocks inside some cells of the mesh in order to regain accuracy. The idea of reconstructing an initial data from the piecewise constant function given by the scheme is not new. For example, in the MUSCL scheme [27], an in-cell linear reconstruction of the solution is used. It allows to built schemes with second-order accuracy in smooth regions. On the contrary, the discontinuous reconstruction strategy is not built to be precise in smooth areas, but yields to schemes that are exact on isolated shocks. This strategy was introduced in [9]. In the case of scalar

advection, this scheme has an interpretation in terms of down-winding under up-winding constraints, and is originally presented that way in [16]. The case of scalar conservation law has been deeply investigated in [6,21,22] and more recently in [13]. It has been extended to the capture of contact discontinuities in [16] and [5]. In [3,23], the reader can find other nondiffusive schemes based on discontinuous reconstructions. The ENO scheme with subcell resolution [19] is also based on a discontinuous reconstruction; this is the only other scheme we know which is also exact on isolated shocks. In parallel to this work, this type of discontinuous reconstruction strategy has been applied to gas dynamics in Eulerian coordinates in [2], and to a scalar equation and a system arising in nonlinear elastodynamics in which under compressive shocks appear, see [1,9] respectively. Compared to [1,2], the main difference with the present paper is that the discontinuous reconstruction strategy is based on the use of an exact Riemann solver, which is numerically costly. Here, we extend the discontinuous reconstruction strategy to the use of an approximate Riemann solver and to the gas dynamics equations in Lagrangian coordinates.

Regarding the second point, *i.e.* the definition of a suitable approximate Riemann solver in order to avoid the costly exact resolution of Riemann problems, we use the approximate solver proposed in [11]. Up to our knowledge, this is the first (and only) entropy consistent approximate Riemann solver which is exact for isolated shock waves. This is the key property an approximate Riemann solver should have to be successfully coupled with the discontinuous reconstruction strategy. This is exactly what we propose to do in the present paper.

Using these tools together allows us to derive numerical schemes that are very precise near shocks. In particular, they have the new property of being exact when the initial data is an isolated shock wave. In order to improve the accuracy of these schemes in smooth regions, a classical MUSCL-Hancock strategy is developed. Moreover, it is important to notice that the proposed numerical schemes do not satisfy the validity of a discrete entropy inequality, despite the facts that the Riemann solver does satisfy an entropy inequality and the in-cell reconstruction procedure is concerned with entropy-satisfying shocks only. Indeed, we will observe that the reconstruction procedure may increase the entropy, but does not prevent the schemes from converging to the correct solution (and in particular does not create non physical shocks).

The paper is organized as follows. The derivation of the scheme is detailed in the first section. More precisely, we describe the approximate Riemann solver introduced in [11] and the proposed in-cell discontinuous reconstruction strategy. Then we put these tools together and present the numerical fluxes. We prove in Subsection 2.4 that the scheme is exact whenever the initial data is an admissible isolated shock. In Section 3 we present some 1-dimensional simulations showing that the scheme has a very low numerical dissipation. In the third and last section, we extend the scheme to 2-dimensional situations by the mean of a directional splitting.

2. Construction of the scheme

Let us start with a short discussion on the usual approximate Riemann solvers (abbreviated ARS in the sequel) and the reason why they are not exact for isolated shock waves. We consider here the Suliciu relaxation procedure [25] (see also [8]), but the same applies to most of the ARS available in the literature. The Suliciu ARS is also the starting point to the solver proposed in [11] and used in the present paper. The idea is to approach the solutions of (1.1) by the solutions of a larger but simpler system, namely

$$\begin{cases} \partial_t \tau - \partial_x u = 0, \\ \partial_t u + \partial_x \pi = 0, \\ \partial_t \mathcal{T} = \frac{1}{\epsilon}(\tau - \mathcal{T}), \end{cases} \tag{2.1}$$

where π is related to the pressure p *via* the expansion

$$\pi = \pi(\mathcal{T}) = p(\mathcal{T}) + a^2(\mathcal{T} - \tau).$$

When ϵ tends to 0, we recover asymptotically the p-system (1.1) we are interested in. For stability reason a must be chosen larger than the maximum speed of the wave appearing in the initial system (1.1), see the next section and [7,10,12,14,20] for more details. This is the so-called subcharacteristic stability condition.

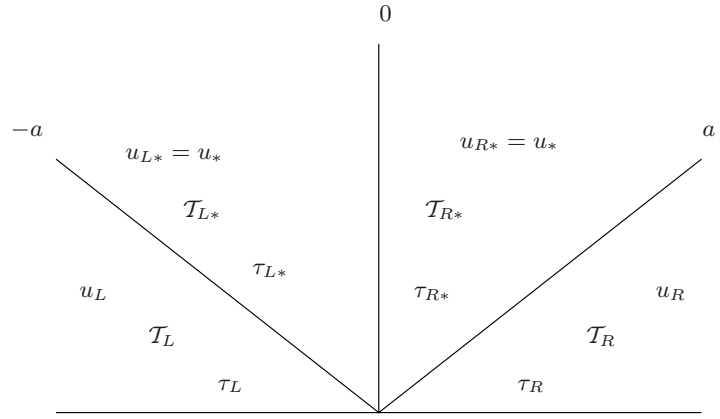

FIGURE 1. The approximate Riemann solver of Suliciu.

System (2.1) is actually simpler to solve than the original p-system (1.1) since the Riemann problem associated to (2.1), namely

$$\begin{cases} \partial_t \tau - \partial_x u = 0, \\ \partial_t u + \partial_x \pi = 0, \\ \partial_t \mathcal{T} = 0, \\ (\tau, u, \mathcal{T})(t = 0, x) = (\tau_L, u_L, \mathcal{T}_L)\mathbf{1}_{x<0} + (\tau_R, u_R, \mathcal{T}_R)\mathbf{1}_{x\geq 0}, \\ \mathcal{T}_L = \tau_L \quad \text{and} \quad \mathcal{T}_R = \tau_R, \end{cases} \tag{2.2}$$

where the initial data is taken at equilibrium, can be explicitly solved. The characteristic fields are easily shown to be linearly degenerate, and the solution of (2.2) contains three contact discontinuities, propagating with velocities $-a$, 0, and a. We denote by $(\tau_{L,*}, u_{L,*}, \mathcal{T}_{L,*})$ the state on the left of the stationary wave, and by $(\tau_{R,*}, u_{R,*}, \mathcal{T}_{R,*})$ the state on its right (see Fig. 1). The notation are similar for the other quantities, and in particular $p_L = p(\tau_L) = \pi_L$ and $p_R = p(\tau_R) = \pi_R$.

The intermediate states can be obtained using the Rankine–Hugoniot relations across each contact discontinuities, and are given by

$$\begin{cases} u_* := u_{L*} = u_{R*} = \frac{u_L + u_R}{2} - \frac{\pi_R - \pi_L}{2a}, \\ \pi_* := \pi_{L*} = \pi_{R*} = \frac{\pi_L + \pi_R}{2} - \frac{a}{2}(u_R - u_L), \\ \tau_{L*} = \tau_L + \frac{u_* - u_L}{a}, \\ \tau_{R*} = \tau_R - \frac{u_* - u_R}{a}, \\ \mathcal{T}_{L*} = \tau_L, \\ \mathcal{T}_{R*} = \tau_R. \end{cases} \tag{2.3}$$

We refer once again to [17] for details. Importantly, since a is chosen larger than any speed of propagation of (1.1) for stability reasons, there is no hope to capture exactly isolated shocks with any Godunov-type method using this approximate Riemann solver.

2.1. An exact approximate Riemann solver on isolated shock waves

In this section we briefly describe the approximate Riemann solver introduced in [11] to solve (1.1)–(1.3) and refer to this paper for details. The idea of [11] is to modify the approximate Riemann solver given by (2.2) by introducing a new wave propagating with a velocity σ in order for the new ARS to be exact on isolated shock waves. The new wave pattern is depicted on Figure 2. Attached to this new wave is a parameter θ, which makes the link between the case of an isolated shock ($\theta = 1$, the other three waves are trivial) and the classical solver

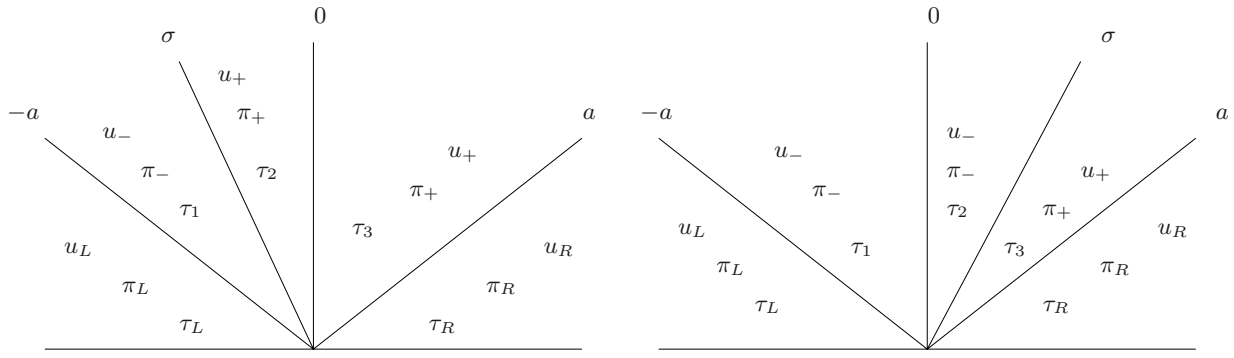

FIGURE 2. Structure of the Riemann solution depending on the sign of σ.

($\theta = 0$, the new wave is trivial and the solver coincides with (2.3)). Moreover, this parameter can be chosen in such a way that the new ARS is entropy satisfying and exact on isolated shocks. In other words, the parameter θ can be seen as a detection parameter for shocks. We also refer the reader to the recent paper [15] for a similar approach and a convergence proof.

The proposed approximate solution is the exact solution of the following system with Riemann initial data at equilibrium:

$$\begin{cases} \partial_t \tau - \partial_x u = 0, \\ \partial_t u + \partial_x \pi(\mathcal{T}) = 0, \\ \partial_t \mathcal{T} = \mathcal{M}(\theta)\delta_{x=\sigma t}, \\ (\tau, u, \mathcal{T})(t=0,x) = (\tau_L, u_L, \mathcal{T}_L)\mathbf{1}_{x<0} + (\tau_R, u_R, \mathcal{T}_R)\mathbf{1}_{x>0}, \\ \mathcal{T}_L = \tau_L \quad \text{and} \quad \mathcal{T}_R = \tau_R. \end{cases} \tag{2.4}$$

System (2.4) is a modified version of (2.1), where the measure valued right hand side $\mathcal{M}(\theta)\delta_{x=\sigma t}$ allows the solution to jump along the line $x = \sigma t$. The parameter σ is chosen such that if the initial datum is an isolated shock, σ is the exact speed of this shock. The Rankine–Hugoniot relations (1.4) yield

$$s^2 = -\frac{p_L - p_R}{\tau_L - \tau_R}.$$

In [11] the authors then propose to set

$$\sigma = \operatorname{sign}(\tau_R - \tau_L)\sqrt{-\frac{p_L - p_R}{\tau_L - \tau_R}}, \tag{2.5}$$

the role of the sign function is to distinguish in between entropy shocks of the first (resp. the second) eigenvalue $-\sqrt{-p'}$ (resp. $\sqrt{-p'}$), for which the shock has a negative velocity and $\tau_R < \tau_L$ (resp. a positive velocity and $\tau_R > \tau_L$). The parameter θ will be chosen such that the approximate Riemann solver is entropy satisfying and exact on isolated shockwaves.

The solution of System (2.4) has four waves, namely the three usual waves having speeds $-a$, 0 and a, and a wave which propagates at speed σ driven by the source term. According to [11], this σ-wave has to be understood as an approximation of the shock wave with the largest amplitude in the exact Riemann solution of (1.1)–(1.3). This approximation turns out to be exact in the case of an isolated shock wave. The structure of the new ARS is depicted on Figure 2.

To define the three intermediate states (and hence the nine unknowns), consistency relations and Rankine–Hugoniot relations are imposed by the authors in [11]. We note in particular that u and π are constant through the stationary wave while the quantity denoted by:

$$\mathcal{I} = \pi(\mathcal{T}) + a^2\tau = p(\mathcal{T}) + a^2\mathcal{T} \tag{2.6}$$

is constant through the $-a$- and a-waves. We denote with a minus subscript (resp. a plus subscript) their values on the left (resp. on the right) of the σ-wave. The intermediate states are found by solving a linear system (in τ, u and $\mathcal{I}$) and are given, when $\sigma > 0$, by

$$\begin{cases} u_- &= u_* + \frac{\sigma\theta}{2a}(a-\sigma)(\tau_R - \tau_L), \\ u_+ &= u_* - \frac{\sigma\theta}{2a}(a+\sigma)(\tau_R - \tau_L), \\ \tau_1 &= \tau_L + \frac{1}{a}(u_- - u_L), \\ \tau_3 &= \tau_R + \frac{1}{a}(u_R - u_+), \\ \tau_2 &= \tau_3 - \theta(\tau_R - \tau_L), \end{cases} \quad \text{and} \quad \begin{cases} \pi_- &= \pi_* - \frac{\sigma\theta}{2}(a-\sigma)(\tau_R - \tau_L), \\ \pi_+ &= \pi_* - \frac{\sigma\theta}{2}(a+\sigma)(\tau_R - \tau_L), \\ \mathcal{I}_1 &= \mathcal{I}_L, \\ \mathcal{I}_2 &= (1-\theta)\mathcal{I}_R + \theta\mathcal{I}_L, \\ \mathcal{I}_3 &= \mathcal{I}_R. \end{cases} \tag{2.7}$$

and when $\sigma < 0$, by

$$\begin{cases} u_- &= u_* + \frac{\sigma\theta}{2a}(a-\sigma)(\tau_R - \tau_L), \\ u_+ &= u_* - \frac{\sigma\theta}{2a}(a+\sigma)(\tau_R - \tau_L), \\ \tau_1 &= \tau_L + \frac{1}{a}(u_- - u_L), \\ \tau_3 &= \tau_R + \frac{1}{a}(u_R - u_+), \\ \tau_2 &= \tau_1 + \theta(\tau_R - \tau_L), \end{cases} \quad \text{and} \quad \begin{cases} \pi_- &= \pi_* - \frac{\sigma\theta}{2}(a-\sigma)(\tau_R - \tau_L), \\ \pi_+ &= \pi_* - \frac{\sigma\theta}{2}(a+\sigma)(\tau_R - \tau_L), \\ \mathcal{I}_1 &= \mathcal{I}_L, \\ \mathcal{I}_2 &= (1-\theta)\mathcal{I}_L + \theta\mathcal{I}_R, \\ \mathcal{I}_3 &= \mathcal{I}_R. \end{cases} \tag{2.8}$$

The states denoted with a star subscript correspond to intermediate states in the Suliciu ARS. Their expressions have been given in (2.3).

The key point of [11] is to pick θ is such a way that the solver satisfies a discrete entropy inequality and gives the exact solution when the initial data is an isolated shock propagating with speed s (in which case $\sigma = s$ thanks to (2.5)). Under the classical subcharacteristic condition

$$|a| > \max_{\tau \in \{\tau_L, \tau_{L*}, \tau_{R*}, \tau_R\}} \sqrt{-p'(\tau)}, \tag{2.9}$$

it can be achieved with the choice

$$\begin{aligned} \sigma\theta(\mathcal{I}_R - \mathcal{I}_L) = \max\Big(0, \min\Big(&\sigma(\mathcal{I}_R - \mathcal{I}_L), -2a(a^2-\sigma^2)\mathcal{A}(v_L, v_R), \\ &\frac{a^2|\sigma|(a+|\sigma|)}{a+|\sigma|/2}(\tau_{R*} - \tau_{L*})\mathrm{sign}(\sigma)\Big)\Big), \end{aligned} \tag{2.10}$$

where

$$\mathcal{A}(v_L, v_R) = \frac{\int^{\tau_R} p(s)\,\mathrm{d}s + \frac{\pi_R}{2a^2} - \int^{\tau_L} p(s)\,\mathrm{d}s - \frac{\pi_L}{2a^2}}{\mathcal{I}_R - \mathcal{I}_L} - \frac{\pi_*}{a^2}.$$

We recall below the main result of [11].

Theorem 2.1. *Under the subcharacteristic condition (2.9), the approximate Riemann solver defined by (2.5), (2.7), (2.8) and (2.10) is conservative and entropy satisfying, preserves the phase space Ω, is Lipschitz continuous with respect to the initial Riemann data, and is exact on isolated shocks (which, again, means that if the initial condition is such that the exact solution is an isolated entropy shock wave, the proposed approximate solution coincides with the exact one).*

2.2. Discontinuous reconstruction schemes

This approximate Riemann solver will be coupled with the discontinuous reconstruction strategy introduced in [9] on the scalar conservation law with increasing flux, and extended in [2] to the system case of the Euler equations using exact Riemann solvers. The aim of the discontinuous reconstruction strategy is to obtain non-diffusive conservative finite volume schemes, which moreover are exact for isolated and admissible shock waves. Let us first recall the formulation of finite volume schemes on a moving grid. We denote by $t^0 = 0 < t^1 < t^2 < \dots$

the time discretization and by $\Delta t^n = t^{n+1} - t^n$ the nth time step. The real line is divided with cells that are always of length Δx but the cells will move at each time step. In the sequel we will also propose a scheme on a fixed grid, but for the sake of clarity it seemed more natural to us to begin with a (fixed-size) moving grid. We denote by x_j^0 the centers of the cells at time t^0 and by $x_{j+1/2}^0 = x_j^0 + \Delta x/2$ their extremities. At the nth iteration, a mesh velocity V_{mesh}^n is given, and the mesh moves from time to time according to the mesh velocity: $x_j^{n+1} = x_j^n + \Delta t^n\, V_{\text{mesh}}^n$, and accordingly $x_{j+1/2}^{n+1} = x_j^{n+1} + \frac{\Delta x}{2}$. We denote by $U = (\tau, u)$ the vector of conservative variables and by $F(U) = (-u, p(\tau))$ the flux. Integrating equation (1.1) on the space-time slab

$$\left\{(t,x) \in \mathbb{R}_+ \times \mathbb{R} :\ t^n \le t < t^{n+1},\ x_{j-1/2}^n + V_{\text{mesh}}^n (t - t^n) \le x < x_{j+1/2}^n + V_{\text{mesh}}^n (t - t^n)\right\},$$

we obtain the scheme

$$U_j^{n+1} = U_j^n - \frac{\Delta t^n}{\Delta x}(\mathcal{F}_{j+1/2}^n - \mathcal{F}_{j-1/2}^n), \tag{2.11}$$

where $U_j^n = (\tau_j^n, u_j^n)$ is supposed to be an approximation of the mean value of the exact solution at time t^n on the jth cell:

$$U_j^n \approx \frac{1}{\Delta x} \int_{x_{j-1/2}^n}^{x_{j+1/2}^n} U(t^n, x)\, \mathrm{d}x,$$

and the numerical flux $\mathcal{F}_{j+1/2}^n = (\mathcal{F}_{j+1/2}^{n,\tau}, \mathcal{F}_{j+1/2}^{n,u})$ is an approximation of the exact flux along the line $x_{j+1/2}^n + V_{\text{mesh}}^n (t - t^n)$, namely

$$\begin{aligned}\mathcal{F}_{j+1/2}^n \approx \frac{1}{\Delta t^n} \int_{t^n}^{t^{n+1}} & F(U(s, x_{j+1/2}^n + V_{\text{mesh}}^n (s - t^n))) \\ & - V_{\text{mesh}}^n U(s, x_{j+1/2}^n + V_{\text{mesh}}^n (s - t^n))\, \mathrm{d}s.\end{aligned}$$

The choice of a formula expressing $\mathcal{F}_{j+1/2}^n$ as a function of the mean values $(U_k^n)_{k\in\mathbb{Z}}$ defines the finite volume scheme. In the discontinuous reconstruction scheme presented below, the numerical flux $\mathcal{F}_{j+1/2}^n$ will depend on $(U_k^n)_{k\in\{j-1,j,j+1\}}$ when V_{mesh}^n is nonpositive and on $(U_k^n)_{k\in\{j,j+1,j+2\}}$ when V_{mesh}^n is nonnegative. The idea of the scheme is to reconstruct entropy satisfying shocks inside each cell of the mesh, using the neighboring cells, and let them evolve during a time Δt^n to compute the flux. The use of a moving grid is crucial to avoid to deal with waves interactions, but as already stated, a natural version of the scheme on fixed grids will be proposed as well.

Let us first address the CFL restriction on the time step Δt and let us then describe precisely the derivation of the discontinuous reconstruction scheme based on the ARS described in the previous section.

Moving mesh and CFL condition

For all integer j, we solve the Riemann problem $(\mathcal{R}_j)$ for the augmented system (2.4), with initial data at equilibrium

$$(\tau_L, u_L, \mathcal{T}_L) = (\tau_{j-1}^n, u_{j-1}^n, \tau_{j-1}^n) \quad \text{and} \quad (\tau_R, u_R, \mathcal{T}_R) = (\tau_{j+1}^n, u_{j+1}^n, \tau_{j+1}^n), \tag{2.12}$$

i.e. involving the neighboring cells $[x_{j-3/2}^n, x_{j-1/2}^n]$ and $[x_{j+1/2}^n, x_{j+3/2}^n]$.

We denote by $\pm a_j^n$ the speed of the extremal waves, such that (2.9) holds true, and by σ_j^n the speed of the additional wave (in accordance with the notation of Fig. 2). We denote by $(u_{j,-}^n, u_{j,+}^n, \pi_{j,-}^n, \pi_{j,+}^n, \tau_{j,1}^n, \tau_{j,2}^n, \tau_{j,3}^n)$ the intermediate states appearing in the solution, defined by (2.7) or (2.8) (depending on the sign of σ_j^n), with (2.12) for the left and right states. Then, we fix a mesh velocity V_{mesh}^n such that

$$|V_{\text{mesh}}^n| \ge V_{\text{waves}}^n := \max_{k\in\mathbb{Z}} a_k^n. \tag{2.13}$$

The time step Δt is constrained by the CFL condition

$$\Delta t^n \le \frac{\Delta x}{(|V_{\text{mesh}}^n| + V_{\text{waves}}^n)}. \tag{2.14}$$

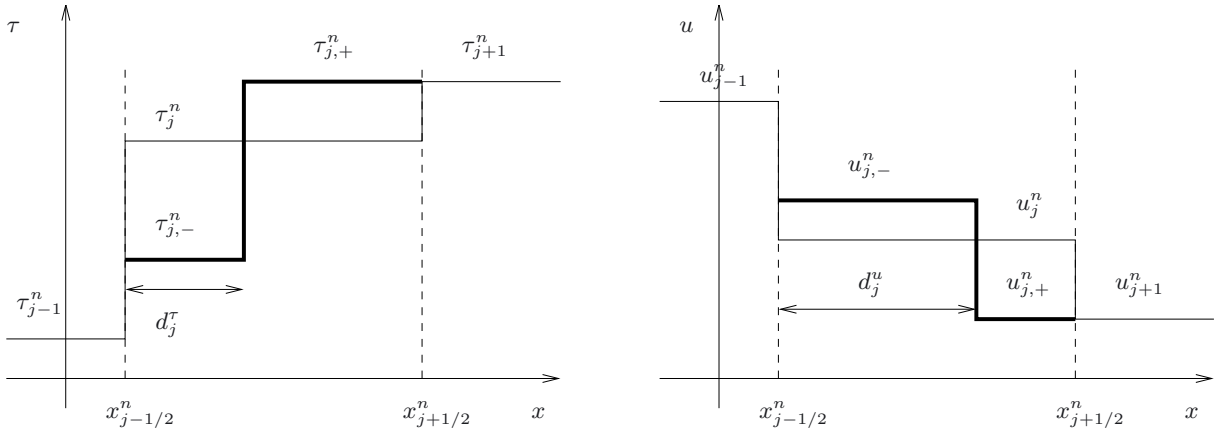

FIGURE 3. Reconstruction of a shock in the jth cell.

Conditions (2.13) and (2.14) ensure the following facts, that will be widely used in the sequel.

- A wave emitted at time t^n at point $x^n_{j+1/2}$ will not cross the interface $x = x^n_{j+1/2} + V^n_{\text{mesh}}(t - t^n)$ by (2.13). By (2.14), it will not cross the neighboring interfaces $x = x^n_{j-1/2} + V^n_{\text{mesh}}(t - t^n)$ and $x = x^n_{j+3/2} + V^n_{\text{mesh}}(t - t^n)$ within the time step either.
- More generally, a wave emitted somewhere in the cell $[x^n_{j-1/2}, x^n_{j+1/2}]$ at time t^n can only cross the interface $x = x^n_{j+1/2} + V^n_{\text{mesh}}(t - t^n)$ if $V^n_{\text{mesh}} < 0$ and the interface $x = x^n_{j-1/2} + V^n_{\text{mesh}}(t - t^n)$ if $V^n_{\text{mesh}} > 0$.
- If a wave emitted in the jth cell interacts with a wave emitted in the $(j + 1)$th cell this interaction occurs inside a cell and the waves created by this interaction stay in that cell and do not interact with the interface $x = x^n_{j+1/2} + V^n_{\text{mesh}}(t - t^n)$. This last point is true for scalar conservation laws, because the velocity of the waves is smaller after the interaction than before. When considering systems of conservation law s, this velocity can increase, so that it is wiser to overestimate V^n_{mesh} at least for the first iterations in time.

In practice, for some μ in $(0, 0.5)$ referred to as the courant number, we take

$$\Delta t^n = \frac{\mu \Delta x}{V^n_{\text{waves}}},$$

and $V^n_{\text{mesh}} = (-1)^n \frac{\Delta x}{2\Delta t^n}$. Conditions (2.13) and (2.14) are fulfilled with this choice and we have $x^{n+1}_j = x^n_j + \frac{(-1)^n \Delta x}{2}$. Note that the mesh moves alternatively with positive and negative speeds and has always cells of size Δx.

Reconstruction of shocks

We denote by $U^n_{j,-} = (\tau^n_{j,-}, u^n_{j,-})$ and $U^n_{j,+} = (\tau^n_{j,+}, u^n_{j,+})$ the states around the σ^n_j-wave in the Riemann problem $(\mathcal{R}_j)$ (see Fig. 2 for the link between $\tau_\pm$ and τ_1, τ_2, τ_3 in formula (2.7) and (2.8)). The core of the discontinuous reconstruction strategy is to see the mean value U^n_j as the average of a shock between the state $U^n_{j,-}$ and the state $U^n_{j,+}$, located somewhere in the cell $[x^n_{j-1/2}, x^n_{j+1/2}]$ and propagating with velocity σ^n_j. This process and the notation are illustrated on Figure 3.

If we use the conservation of τ at time t^n on the cell $[x^n_{j-1/2}, x^n_{j+1/2}]$ to locate the reconstructed shock, we obtain that it should lie at a distance $d^{n,\tau}_j$ of $x^n_{j-1/2}$ such that

$$d^{n,\tau}_j \tau^n_{j,-} + (\Delta x - d^{n,\tau}_j)\tau^n_{j,+} = \Delta x \tau^n_j,$$

which yields

$$d_j^{n,\tau} = \Delta x \frac{\tau_{j,+}^n - \tau_j^n}{\tau_{j,+}^n - \tau_{j,-}^n}. \tag{2.15}$$

Similarly, if we use the conservation of u, we obtain that it should lie at the distance

$$d_j^{n,u} = \Delta x \frac{u_{j,+}^n - u_j^n}{u_{j,+}^n - u_{j,-}^n} \tag{2.16}$$

of $x_{j-1/2}^n$. The two distances $d_j^{n,\tau}$ and $d_j^{n,u}$ are different in general, but we will see later on that they do coincide in the case of an isolated shock wave. If one of those distances is outside of the interval $(0, \Delta x)$, we consider that the mean value in cell j does not come from the average of a shock, and we do not perform any reconstruction within the cell $[x_{j-1/2}^n, x_{j+1/2}^n]$. It yields the following definition.

Definition 2.2. The left and right reconstructed states in the jth cell at time t^n, $(\tau_{j,L}^n, u_{j,L}^n)$ and $(\tau_{j,R}^n, u_{j,R}^n)$, are defined as follow:

$$(\tau_{j,L}^n, u_{j,L}^n) = \begin{cases} (\tau_{j,-}^n, u_{j,-}^n) & \text{if } d_j^{n,\tau} \in [0, \Delta x] \text{ and } d_j^{n,u} \in [0, \Delta x], \\ (\tau_j^n, u_j^n) & \text{otherwise,} \end{cases} \tag{2.17}$$

and

$$(\tau_{j,R}^n, u_{j,R}^n) = \begin{cases} (\tau_{j,+}^n, u_{j,+}^n) & \text{if } d_j^{n,\tau} \in [0, \Delta x] \text{ and } d_j^{n,u} \in [0, \Delta x], \\ (\tau_j^n, u_j^n) & \text{otherwise.} \end{cases} \tag{2.18}$$

Computation of the fluxes

The fluxes are computed by letting the reconstructed shocks evolve during the time Δt^n. To illustrate the interest of using a moving mesh, consider the case in Figure 4, where a 2-shock is reconstructed in the cell $[x_{j-1/2}^n, x_{j+1/2}^n]$ and a 1-shock is reconstructed in the cell $[x_{j+1/2}^n, x_{j+3/2}^n]$ ($\sigma_j^n > 0$ and $\sigma_{j+1}^n < 0$). At time t^n, both shocks are located near $x_{j+1/2}^n$, and they will interact within the time step. As it can be seen on Figure 4, it is impossible to compute the flux on the interface $x = x_{j+1/2}^n$ (blue bold vertical line) without resolving the wave interaction. On the other hand, computing the flux along the interface $x = x_{j+1/2} + V_{\text{mesh}}^n(t - t^n)$ (dashed line) is much easier. Under conditions (2.13) and (2.14), this flux is piecewise constant and its computation only requires the knowledge of the crossing time between the shock reconstructed in cell j when $V_{\text{mesh}}^n < 0$ (in cell $j+1$ when $V_{\text{mesh}}^n > 0$) and the interface. Let us focus on the case where V_{mesh}^n is negative. The two components of the flux are computed in the same way, except that the position of the reconstructed shock in the jth cell at the beginning of the time step is different for each conserved variable. More precisely, in order to compute the flux in τ, we consider that the shock reconstructed in cell $[x_{j-1/2}^n, x_{j+1/2}^n]$ is initially located at the distance $d_j^{n,\tau}$ of $x_{j-1/2}^n$. We recall that this ensures the conservation of τ inside the jth cell. As V_{mesh}^n is negative, the reconstructed shock crosses the right interface $x = x_{j+1/2}^n + V_{\text{mesh}}^n(t - t^n)$ at the time $t^n + T_j^{n,\tau}$, where $T_j^{n,\tau}$ verifies (whatever the sign of σ_j^n is)

$$x_{j-1/2}^n + d_j^{n,\tau} + \sigma_j^n T_j^{n,\tau} = x_{j+1/2}^n + V_{\text{mesh}}^n T_j^{n,\tau},$$

i.e.

$$T_j^{n,\tau} = \frac{\Delta x - d_j^{n,\tau}}{\sigma_j^n - V_{\text{mesh}}^n}. \tag{2.19}$$

As we already explained, under conditions (2.13) and (2.14), the only wave that can cross the interface $x = x_{j+1/2}^n + V_{\text{mesh}}^n(t - t^n)$ during the time step is the shock reconstructed in the jth cell. Thus the flux passing through this interface (red dashed line on Fig. 4) is simply $-u_{j,R} - V_{\text{mesh}}^n \tau_{j,R}^n$ before the crossing time $t^n + T_j^{n,\tau}$

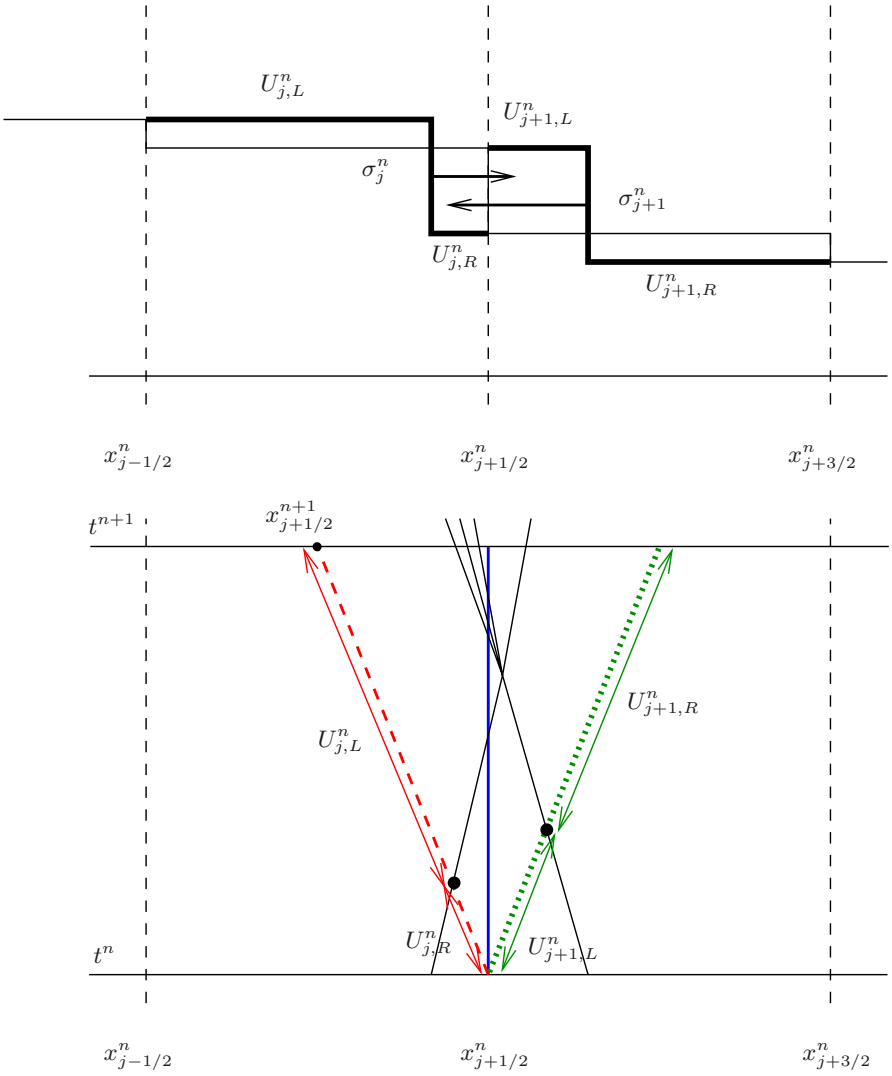

FIGURE 4. *Top*: Reconstruction of a 1-shock in the jth cell ($\sigma^n_j > 0$) and of a 2-shock in the $(j+1)$th cell ($\sigma^n_{j+1} < 0$). *Bottom*: In black, positions of the reconstructed shocks through time, and the waves emitted when they interact. It is easy to compute the flux through the red dashed and green dotted interfaces, but not through the blue bold vertical one. (Color online)

and $-u_{j,L} - V^n_{\text{mesh}}\tau^n_{j,L}$ after it. Of course, $T^{n,\tau}_j$ can be larger than Δt^n, in which case the flux is $-u_{j,R} - V^n_{\text{mesh}}\tau^n_{j,R}$ during the whole time step. Eventually the flux in τ writes

$$\begin{aligned}\Delta t^n \mathcal{F}^{n,\tau}_{j+1/2} = &\left(-u^n_{j,R} - V^n_{\text{mesh}}\tau^n_{j,R}\right)\min(\Delta t^n, T^{n,\tau}_j)\\ &+ \left(-u^n_{j,L} - V^n_{\text{mesh}}\tau^n_{j,L}\right)(\Delta t^n - \min(\Delta t^n, T^{n,\tau}_j)).\end{aligned}$$

To compute the flux in the u variable, the only difference is that the shock reconstructed in the jth cell is initially located at the distance $d_j^{n,u}$ of $x_{j+1/2}^n$, using the conservation of u instead of τ. Thus the crossing time is $t^n + T_j^{n,u}$ with

$$T_j^{n,u} = \frac{\Delta x - d_j^{n,u}}{\sigma_j^n - V_{\text{mesh}}^n},$$

and we obtain similarly the second component of the numerical flux. Finally if V_{mesh}^n is negative we have

$$\begin{aligned}
\Delta t^n \mathcal{F}_{j+1/2}^{n,\tau} &= \left(-u_{j,R}^n - V_{\text{mesh}}^n \tau_{j,R}^n\right) \min(\Delta t^n, T_j^{n,\tau}) \\
&\quad + \left(-u_{j,L}^n - V_{\text{mesh}}^n \tau_{j,L}^n\right) (\Delta t^n - \min(\Delta t^n, T_j^{n,\tau})), \\
\Delta t^n \mathcal{F}_{j+1/2}^{n,u} &= \left(\pi_{j,R}^n - V_{\text{mesh}}^n u_{j,R}^n\right) \min(\Delta t^n, T_j^{n,u}) \\
&\quad + \left(\pi_{j,L}^n - V_{\text{mesh}}^n u_{j,L}^n\right) (\Delta t^n - \min(\Delta t^n, T_j^{n,u})).
\end{aligned} \tag{2.20}$$

If V_{mesh}^n is positive, the only wave that can cross the interface $x = x_{j+1/2}^n + V_{\text{mesh}}^n(t - t^n)$ during the time step is the shock reconstructed in cell $j+1$, which propagates with velocity σ_{j+1}^n. In the variables τ and u respectively, it needs a time

$$T_{j+1}^{n,\tau} = \frac{d_{j+1}^{n,\tau}}{V_{\text{mesh}}^n - \sigma_{j+1}^n} \quad \text{or} \quad T_{j+1}^{n,u} = \frac{d_{j+1}^{n,u}}{V_{\text{mesh}}^n - \sigma_{j+1}^n}$$

to cross the interface. In that case, the flux $\mathcal{F}_{j+1/2}^n$ passing through the interface is once again piecewise constant, but this time is computed with $U_{j+1,L}^n$ before the crossing time, and with $U_{j+1,R}^n$ after it (green dotted interface on Fig. 4). It writes

$$\begin{aligned}
\Delta t^n \mathcal{F}_{j+1/2}^{n,\tau} &= \left(-u_{j+1,L}^n - V_{\text{mesh}}^n \tau_{j+1,L}^n\right) \min(\Delta t^n, T_{j+1}^{n,\tau}) \\
&\quad + \left(-u_{j+1,R}^n - V_{\text{mesh}}^n \tau_{j+1,R}^n\right) (\Delta t^n - \min(\Delta t^n, T_{j+1}^{n,\tau})), \\
\Delta t^n \mathcal{F}_{j+1/2}^{n,u} &= \left(\pi_{j+1,L}^n - V_{\text{mesh}}^n u_{j+1,L}^n\right) \min(\Delta t^n, T_{j+1}^{n,u}) \\
&\quad + \left(\pi_{j+1,R}^n - V_{\text{mesh}}^n u_{j+1,R}^n\right) (\Delta t^n - \min(\Delta t^n, T_{j+1}^{n,u})).
\end{aligned} \tag{2.21}$$

Finally, the conservative variables are updated with (2.11).

Remark 2.3. When no reconstruction is performed, *i.e.* when $U_{j,L}^n = U_{j,R}^n = U_j^n$, we have, whatever the values of d_j^n, σ_j^n and T_j^n are,

$$\begin{cases} \mathcal{F}_{j+1/2}^n = F(U_j^n) - V_{\text{mesh}}^n U_j^n & \text{if } V_{\text{mesh}}^n < 0, \\ \mathcal{F}_{j-1/2}^n = F(U_{j+1}^n) - V_{\text{mesh}}^n U_{j+1}^n & \text{if } V_{\text{mesh}}^n > 0. \end{cases}$$

In other words in that case, the numerical fluxes (2.20) and (2.21) coincide with the Lax–Friedrichs scheme on a moving grid, which is well-known to be stable under conditions (2.13) and (2.14).

On a fixed grid

In this section we present a discontinuous reconstruction scheme on a fixed grid. In this section only we take $x_{j+1/2}^{n+1} = x_{j+1/2}^n$ and thus $V_{\text{mesh}}^n = 0$. There is at least three advantages in using a fixed grid:

- the Courant number can be taken in $(0, 1)$, instead of in $(0, 0.5)$ with a moving grid. Thus we can use time steps that are twice larger;
- at equal Courant number in smooth regions, the scheme on a fixed grid is a little less diffusive than on a moving grid. Note that in a similar way, the well-known Rusanov scheme, which can be interpreted in terms of a moving grid as proposed here, is more diffusive than Godunov's scheme.

- dealing with boundary conditions is easier since the domain is fixed here.

The problem is to deal with interactions between reconstructed shocks near an interface. The basic idea is to cancel some reconstructions when it happens. Typically in the example of Figure 4, where two reconstructed shocks cross the blue bold vertical interface within the time step, we decide to cancel those two reconstructions and to use a classical numerical flux. This will be sufficient to obtain the main property of the scheme, namely to be exact when the initial data is an isolated shock.

Introductory discussion

If a shock is reconstructed in the jth cell and has a positive speed ($\sigma_j^n > 0$), it is tempting to use the flux formula (2.20) which gives the flux passing through the $j+1/2$ interface if the initial data were

$$\begin{cases} \tau^0(x) = \tau_{j,L}^n \times \mathbf{1}_{x<x_{j-1/2}^n+d_j^{n,\tau}} + \tau_{j,R}^n \times \mathbf{1}_{x>x_{j-1/2}^n+d_j^{n,\tau}}, \\ u^0(x) = u_{j,L}^n \times \mathbf{1}_{x<x_{j-1/2}^n+d_j^{n,u}} + u_{j,R}^n \times \mathbf{1}_{x>x_{j-1/2}^n+d_j^{n,u}}, \end{cases}$$

(see what happens through the red dashed interface of the bottom of Fig. 4).

However, if a shock is reconstructed in the $j+1$ cell and has a negative speed ($\sigma_{j+1}^n < 0$), it is similarly tempting to use the flux formula (2.21), which gives the flux passing through the $j+1/2$ interface if the initial data were

$$\begin{cases} \tau^0(x) = \tau_{j+1,L}^n \times \mathbf{1}_{x<x_{j+1/2}^n+d_{j+1}^{n,\tau}} + \tau_{j+1,R}^n \times \mathbf{1}_{x>x_{j+1/2}^n+d_{j+1}^{n,\tau}}, \\ u^0(x) = u_{j+1,L}^n \times \mathbf{1}_{x<x_{j+1/2}^n+d_{j+1}^{n,u}} + u_{j+1,R}^n \times \mathbf{1}_{x>x_{j+1/2}^n+d_{j+1}^{n,u}}, \end{cases}$$

(see what happens through the green dotted interface of the bottom of Fig. 4).

In the variable τ, the two shocks interact at time $t^n + T_{j+1/2}^{n,\mathrm{inter},\tau}$ such that

$$d_j^{n,\tau} + \sigma_j^n T_{j+1/2}^{n,\mathrm{inter},\tau} = \Delta x + d_{j+1}^{n,\tau} + \sigma_{j+1}^n T_{j+1/2}^{n,\mathrm{inter},\tau}.$$

We obtain similarly a different interaction time $T_{j+1/2}^{n,\mathrm{inter},u}$ in the variable u. We evaluate the time after which the two shocks interact by

$$T_{j+1/2}^{n,\mathrm{inter}} = \min(T_{j+1/2}^{n,\mathrm{inter},\tau}, T_{j+1/2}^{n,\mathrm{inter},u}) = \min\left(\frac{d_{j+1}^n + \Delta x - d_j^n}{\sigma_j^n - \sigma_{j+1}^n}\right),$$

where the second minimum is taken on the two components of the vectors d_j^n and d_{j+1}^n. The interaction can also occur when σ_j^n and σ_{j+1}^n have the same sign and $\sigma_j^n > \sigma_{j+1}^n$. If this time is smaller than Δt^n, the shocks interact within the time step and the waves created by the resulting interaction are likely to meet the $(j+1/2)$th interface (which was not the case on a moving grid under condition (2.13), see once again Fig. 4). In that case, we do not take into account the reconstructions in cells j and $j+1$, and simply use the Godunov-type flux (associated with (2.4)) instead of the reconstruction flux (2.20) or (2.21).

Definition of the fluxes

Let us now be more precise and introduce some notations. We denote by $\mathcal{F}^{\mathrm{GOD}}(U_L, U_R)$ the Godunov-type scheme associated with the ARS (2.4):

$$\mathcal{F}^{\mathrm{GOD}}(U_L, U_R) = \begin{cases} (-u_-, \pi_-) & \text{if } \sigma > 0, \\ (-u_+, \pi_+) & \text{if } \sigma \le 0, \end{cases} \tag{2.22}$$

(see Fig. 2). We also denote by $\mathcal{F}_{j+1/2}^{n,\leftarrow}$ the flux given by (2.21) and by $\mathcal{F}_{j+1/2}^{n,\rightarrow}$ the flux given by (2.20) (with $V_{\mathrm{mesh}}^n = 0$). Moreover, we use the convention $\sigma_j^n = 0$ if no reconstruction is performed in cell j, and we extend the definition of the interaction time by

$$T_{j+1/2}^{n,\mathrm{inter}} = \begin{cases} \min\left(\frac{d_{j+1}^n + \Delta x - d_j^n}{\sigma_j^n - \sigma_{j+1}^n}\right) & \text{if } \sigma_j^n > \sigma_{j+1}^n, \text{ and } \sigma_{j+1}^n \sigma_j^n \neq 0 \\ +\infty & \text{otherwise.} \end{cases} \tag{2.23}$$

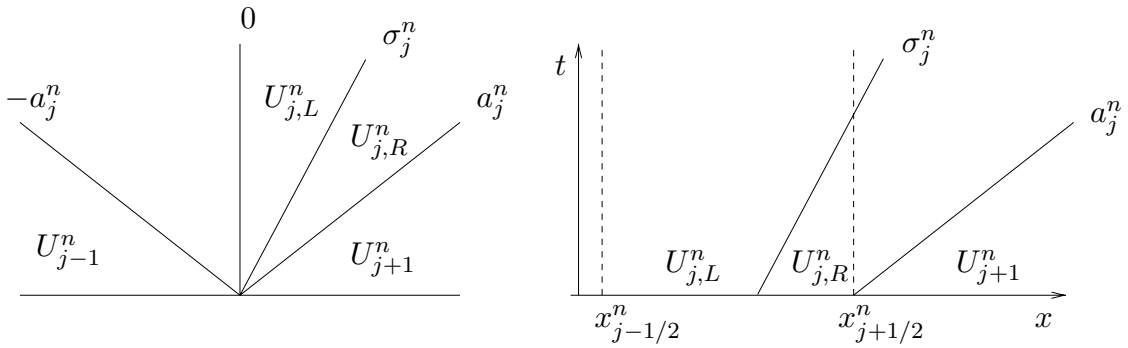

FIGURE 5. *Left*: the structure of the ARS used to determine $U_{j,L}^n$ and $U_{j,R}^n$. *Right*: the waves emitted in the reconstructed solution: there is only a wave at speed a_j^n between $U_{j,R}^n$ and U_{j+1}^n, which is faster than the reconstructed shock. Thus the flux through the interface $j+1/2$ is easily computed and given by $\mathcal{F}_{j+1/2}^{n,\rightarrow}$.

We propose the following fluxes:

$$\mathcal{F}_{j+1/2}^n = \begin{cases} \mathcal{F}_{j+1/2}^{n,\rightarrow} & \text{if } \sigma_j^n > 0,\ T_{j+1/2}^{n,\text{inter}} > \Delta t \text{ and } \sigma_{j+1}^n \geq 0, \\ \mathcal{F}_{j+1/2}^{n,\leftarrow} & \text{if } \sigma_{j+1}^n < 0,\ T_{j+1/2}^{n,\text{inter}} > \Delta t \text{ and } \sigma_j^n \leq 0, \\ \mathcal{F}^{\text{GOD}}(U_j^n, U_{j+1}^n) & \text{if } (\sigma_j^n > 0 \text{ and } \sigma_{j+1}^n < 0) \text{ or } T_{j+1/2}^{n,\text{inter}} \leq \Delta t, \\ \mathcal{F}^{\text{GOD}}(U_{j,R}^n, U_{j+1,L}^n) & \text{otherwise.} \end{cases} \tag{2.24}$$

In particular, for simplicity, we cancel the reconstructions in cells j and $j+1$ if $\sigma_j^n > 0$ and $\sigma_{j+1}^n < 0$.

We now justify the choice of flux $F_{j+1/2}^{n,\rightarrow}$ if $\sigma_j^n > 0$ and $\sigma_{j+1}^n = 0$, which corresponds to the case where a shock with positive speed is reconstructed in the jth cell and no shock is reconstructed in the $(j+1)$th cell. In that case, the approximate Riemann solver (2.4) between the left state U_{jR}^n and the right state U_{j+1}^n has only one nontrivial wave, namely the right extremal one, which has speed a_j^n. This is illustrated on Figure 5. Thus, as $a_j^n > \sigma_j^n$, no wave interaction occurs at interface $j+1/2$. The flux through the interface $j+1/2$ is indeed easily computed and given by $\mathcal{F}_{j+1/2}^{n,\rightarrow}$.

2.3. Coupling the reconstruction scheme with higher order methods

In Remark 2.3, we observed that the reconstruction scheme behaves like the Lax–Friedrichs scheme when no reconstruction is performed. In practice, no reconstruction are performed in smooth areas of the solution, and thus the scheme is very diffusive in those areas, while it is very sharp near shocks (see the numerical simulations in Sects. 3 and 4 below). A simple cure is to use another flux when no reconstruction is performed. In this paper we chose to use a MUSCL-Hancock flux [26], with a minmod slope limiter and the approximate Riemann solver [11]. The flux is computed as follows,

1. The average value U_i^n in cell i at time t^n is replaced by a linear function

$$x \mapsto U_i^n + \frac{\Delta_i^n (x - x_i^n)}{\Delta x},$$

where the slope Δ_i^n is given by

$$\Delta_i^n = \text{minmod}(U_i^n - U_{i-1}^n, U_{i+1}^n - U_i^n)$$

where

$$\text{minmod}(a,b) = \frac{\text{sign}(a) + \text{sign}(b)}{2} \min(|a|, |b|)$$

(other choices are possible, see [26]). We denote by

$$U_{i,L}^{n,MH} = U_i^n - \frac{\Delta_i^n}{2} \quad \text{and} \quad U_{i,R}^{n,MH} = U_i^n + \frac{\Delta_i^n}{2}$$

the boundary extrapolated values.

2. We evolve those boundary extrapolated values for a time $\frac{t^{n+1}-t^n}{2}$ and compute

$$\begin{cases} U_{i,L}^{n+1/2,MH} = U_{i,L}^n + \frac{t^{n+1}-t^n}{2\Delta x}(f(U_{i,L}^{n,MH}) - f(U_{i,R}^{n,MH})), \\ U_{i,R}^{n+1/2,MH} = U_{i,R}^n + \frac{t^{n+1}-t^n}{2\Delta x}(f(U_{i,L}^{n,MH}) - f(U_{i,R}^{n,MH})). \end{cases}$$

3. Eventually, the flux is given by

$$\mathcal{F}_{j+1/2}^{n,MH} = \mathcal{F}_{j+1/2}^{n,GOD}\left(U_{j,R}^{n+1/2,MH}, U_{j+1,L}^{n+1/2,MH}\right).$$

To couple the discontinuous reconstruction scheme with the MUSCL-Hancock flux on a fixed grid, we proceed as follow.

1. We compute the discontinuous reconstruction flux (2.24), and keep in memory the interface that are not concerned by any reconstruction (*i.e.* $\sigma_j^n = 0$ and $\sigma_{j+1}^n = 0$).
2. On those specific interfaces, we use the MUSCL-Hancock flux, with the choice

$$\Delta_i^n = \text{minmod}(U_i^n - U_{i-1,R}^n, U_{i+1,L}^n - U_i^n).$$

2.4. Exact approximation of isolated shocks

We now prove a nontrivial property that states that if the initial data is an isolated admissible shock wave, the discontinuous reconstruction scheme (on a moving or on a fixed grid) is exact. Let us start this section by the following proposition, which is easily verified.

Proposition 2.4. *The numerical fluxes* (2.20) *and* (2.21) (*on a moving grid*) *and* (2.24) (*on a fixed grid*) *are consistent: if* $U_{j-1}^n = U_j^n = U_{j+1}^n = U_{j+2}^n := U$, *then* $\mathcal{F}_{j+1/2}^n = f(U) - V_{\text{mesh}}^n U$ *(we recall that on a fixed grid,* $V_{\text{mesh}}^n = 0$*).*

The aim of this subsection is to prove the following theorem.

Theorem 2.5. *The discontinuous reconstruction scheme is exact whenever the initial data is an isolated entropy satisfying shock. More precisely, suppose that the initial data is*

$$\begin{cases} \tau^0(x) = \tau_L \mathbf{1}_{x<0} + \tau_R \mathbf{1}_{x>0}, \\ u^0(x) = u_L \mathbf{1}_{x<0} + u_R \mathbf{1}_{x>0}, \end{cases}$$

with $u_L > u_R$ *and* (τ_L, u_L) *and* (τ_R, u_R) *linked by the Rankine–Hugoniot relations* (1.4). *Then* U_j^n *is the average of the exact solution at time* t^n *over the interval* $[x_{j-1/2}^n, x_{j+1/2}^n]$ *for all* j *in* $\mathbb{Z}$.

Remark 2.6. In particular, this theorem means that for such particular initial data, no spurious numerical diffusion is created by the scheme. For general initial data, the same behavior is observed, see Section 3 below.

Proof. We prove the result for a 2-shock (the reasoning is identical for a 1-shock), thus in the following we suppose that $\tau_L < \tau_R$. Suppose that the property is verified for an integer n. Then, there exists an integer j_0^n and a distance $d_{j_0^n}^n \in [0, \Delta x]$ such that

$$U_k^n = \begin{cases} U_L & \text{if } k < j_0^n, \\ \frac{d_{j_0^n}}{\Delta x} U_L + \frac{\Delta x - d_{j_0^n}}{\Delta x} U_R & \text{if } k = j_0^n, \\ U_R & \text{if } k > j_0^n. \end{cases}$$

By construction, the approximate Riemann solver of [11] is exact on $(\mathcal{R}_{j_0^n})$. Therefore, the shock is correctly reconstructed in cell j_0^n, and (2.5) ensures that it has the correct speed

$$\sigma := \frac{u_L - u_R}{\tau_R - \tau_L}.$$

The two distances $d^{\tau}_{j_0^n}$ and $d^{u}_{j_0^n}$ given by (2.15) and (2.16) are both equal to $d^n_{j_0^n}$, and correspond to the exact position of the shock at time t^n. On the other hand, no reconstruction is performed in cells $j_0^n - 1$ and $j_0^n + 1$, because it is impossible to have $d^{n,\tau}_{j_0^n-1}$ or $d^{n,\tau}_{j_0^n+1}$ in $(0, \Delta x)$.

Let us indeed explain in detail the case of the cell $j_0^n - 1$. Consider the Riemann problem between the left state (τ_L, u_L) and $(\tilde\tau_R, \tilde u_R) := (\alpha\tau_R + (1-\alpha)\tau_L, \alpha u_R + (1-\alpha)u_L)$, where $\alpha = 1 - \frac{d^n_{j_0^n}}{\Delta x}$. We denote by $\tilde\sigma$ the speed of the shock wave in this Riemann problem, which by (2.5) is given by

$$\tilde\sigma := \sqrt{\frac{p_L - \tilde p_R}{\tilde\tau_R - \tau_L}}, \quad \text{where} \quad \tilde p_R = p(\tilde\tau_R).$$

As $\tau_+ \geq \tau_-$, if τ_- is larger than τ_L, it is impossible to reconstruct τ in cell $j_0^n - 1$ in a conservative manner. We use (2.7) to express the difference $\tau_- - \tau_L$ expresses as a function of θ:

$$\begin{aligned}
\tau_-(\theta) - \tau_L &= \tau_+(\theta) - \theta(\tilde\tau_R - \tau_L) - \tau_L \\
&= \tilde\tau_R + \frac{1}{a}(\tilde u_R - u_+(\theta)) - \theta(\tilde\tau_R - \tau_L) - \tau_L \\
&= (1-\theta)(\tilde\tau_R - \tau_L) + \frac{1}{a}\left(\tilde u_R - u_* + \frac{\tilde\sigma\theta}{2a}(a+\tilde\sigma)(\tilde\tau_R - \tau_L)\right) \\
&= (\tilde\tau_R - \tau_L) + \frac{\tilde u_R - u_*}{a} - \theta(\tilde\tau_R - \tau_L)\left(1 - \frac{\tilde\sigma}{2a^2}(a+\tilde\sigma)\right).
\end{aligned}$$

This function is decreasing with respect to θ. Indeed, $\tilde\tau_R$ is larger than τ_L, and as a is larger than $\tilde\sigma$ by the subcharacteristic condition (2.9), we have

$$\frac{\tilde\sigma(a+\tilde\sigma)}{2a^2} \leq 1.$$

Thus for all θ in $[0,1]$,

$$\tau_-(\theta) - \tau_L \geq \tau_-(\theta = 1) - \tau_L = \frac{1}{a}\left(\tilde u_R - u_* + \frac{\tilde\sigma}{2a}(a+\tilde\sigma)(\tilde\tau_R - \tau_L)\right).$$

Let us prove that the quantity

$$Q := \tilde u_R - u_* + \frac{\tilde\sigma}{2a}(a+\tilde\sigma)(\tilde\tau_R - \tau_L)$$

is positive. Replacing u_* by its value, we obtain

$$Q = \frac{\tilde u_R - u_L}{2} + \frac{\tilde\pi_R - \pi_L}{2a} + \frac{\tilde\sigma}{2a}(a+\tilde\sigma)(\tilde\tau_R - \tau_L).$$

Now, we divide by $\tilde\tau_R - \tau_L$ and use the definition of $\tilde\sigma$ to write

$$\frac{2Q}{\tilde\tau_R - \tau_L} = -\sigma - \frac{\tilde\sigma^2}{a} + \frac{\tilde\sigma}{a}(a+\tilde\sigma) = \tilde\sigma - \sigma.$$

We conclude by remarking that as the pressure is convex,

$$\tilde\pi_R = p(\alpha\tau_R + (1-\alpha)\tau_L) \leq \alpha\pi_R + (1-\alpha)\pi_L$$

and thus

$$\tilde\sigma = \sqrt{\frac{\pi_L - \tilde\pi_R}{\tilde\tau_R - \tau_L}} \geq \sqrt{\frac{\pi_L - \pi_R}{\tau_R - \tau_L}} = \sigma.$$

Proving that no reconstruction is performed in cell j_0^n+1 follows the same lines. We now focus on the Riemann problem between the left state $(\tilde\tau_L,\tilde u_L):=(\alpha\tau_L+(1-\alpha)\tau_R,\alpha u_L+(1-\alpha)u_R)$ and (τ_R,u_R) with $\alpha=d^n_{j_0^n}/\Delta x$. We have

$$\begin{aligned} u_+-u_R &\geq u_*-\frac{\tilde\sigma}{2a}(a+\tilde\sigma)(\tau_R-\tilde\tau_L)-u_R \\ &= \frac{\tilde u_L-u_R}{2}-\frac{\pi_R-\tilde\pi_L}{2a}-\frac{\tilde\sigma}{2a}(a+\tilde\sigma)(\tau_R-\tilde\tau_L) \\ &= \frac{\tau_R-\tilde\tau_L}{2}\left(\sigma+\frac{\tilde\sigma^2}{a}-\frac{\tilde\sigma}{a}(a+\tilde\sigma)\right) \\ &= \frac{\tau_R-\tilde\tau_L}{2}\left(\sigma-\tilde\sigma\right). \end{aligned}$$

It follows that u_+ is larger than u_R, because

$$\tilde\sigma=\sqrt{\frac{\tilde\pi_L-\pi_R}{\tau_R-\tilde\tau_L}}\leq\sqrt{\frac{\pi_L-\pi_R}{\tau_R-\tau_L}}=\sigma.$$

Thus, $\tau_+=\tau_R+\frac{1}{a}(u_R-u_+)$ is smaller than τ_L, and as τ_- is smaller than τ_+, it is impossible to reconstruct τ. The rest of the proof consists in an elementary checking that (2.20) and (2.21) give the correct flux. The case of a fixed grid follows because no reconstruction is cancelled. □

3. One dimensional numerical simulations

In this section we present several numerical simulations to test the non diffusive behavior of the schemes presented in the previous section. The space interval $[-1,1]$ is discretized with 100 cells and the pressure law is $p(\tau)=\tau^{-2}$. We take

$$\Delta t^n=0.45\frac{\Delta x}{V^n_{\text{waves}}}\quad\text{and}\quad V^n_{\text{mesh}}=(-1)^n\frac{\Delta x}{2\Delta t^n},$$

so that both (2.13) and (2.14) hold true. In each case, we compare the discontinuous reconstruction schemes on a moving and on a fixed grid (abbreviated `RecMG` and `RecFG` in the sequel), the Godunov-type scheme and a MUSCL-Hancock scheme, all based on the approximate Riemann solver of [11]. The flux of the "Godunov-type scheme" is computed on a fixed grid ($V^n_{\text{mesh}}=0$) and its expression is given in (2.22).

The first three test cases are taken from [11], the fourth one is a variant of the fast shock of Arora and Roe [4]. On test cases involving only shockwaves, the results given by the reconstruction schemes on moving and fixed grids are very close to each other, and we only show the results given by the scheme on a moving grid. The main difference between the two schemes lies on the fact that the scheme on a fixed grid is a little less diffusive in the smooth areas, see test case 2.

Test 1: Isolated shock

Our first test is the Riemann problem (1.3) with

$$\tau_L=1,\ u_L=0,\ \tau_R=2\quad\text{and}\quad u_R=-\sqrt{3}/2.$$

It corresponds to an isolated shock. Theorem 2.5 is illustrated on Figure 6, namely the shock is perfectly advected by the reconstruction scheme, while it is diffused by the Godunov-type scheme. On the bottom of this figure, we can see that there is only one intermediate value in the shock profile given by the reconstruction scheme, which corresponds to the average of the exact solution on the cell.

Test 2: Rarefaction and shock

For this test case, the initial data is (1.3) with

$$\tau_L=0.3,\ u_L=0,\ \tau_R=0.6\quad\text{and}\quad u_R=0.$$

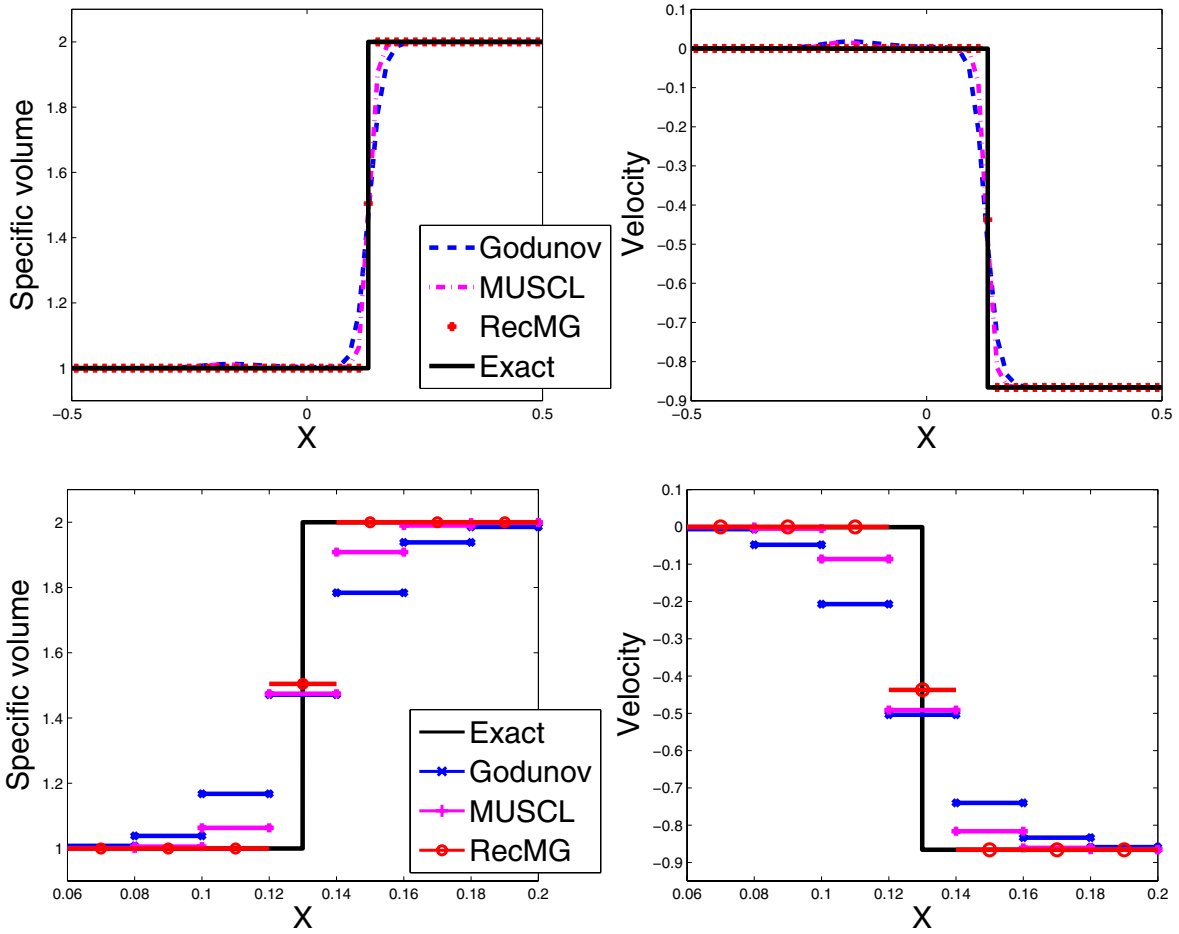

FIGURE 6. Test 1: Specific volume (*top left*) and velocity (*top right*) at time $t = 0.15$. *Bottom*: close-up on the piecewise constant shock profile.

The solution contains a 1-rarefaction wave and a 2-shock. On Figure 7, we can see that the shock is sharply captured by the reconstruction schemes. The comparison in the rarefaction wave shows first, that the reconstruction scheme on a fixed grid is slightly less diffusive than the one on a moving grid, and second, that it has the same amount of diffusion as the Godunov scheme in the smooth areas. This was expected: in the rarefaction the σ-wave is trivial and the fluxes (2.24) and (2.20-2.21) coincide with the Godunov fluxes, see Remark 2.3. In particular the reconstruction scheme in this form is not competitive with the second order MUSCL-Hancock scheme. A simple and computationally affordable cure is to replace the Godunov flux by the MUSCL-Hancock flux at the interfaces which are not concerned by any reconstruction, as explained in Section 2.3. We obtain a new scheme, abbreviated in `Rec+MUSCL` in the legends, which behaves as the reconstruction scheme near the shock and as the MUSCL-Hancock scheme inside the rarefaction. Figure 8 is a zoom around the shock. The slight overshoots are created in the first iterations in time. Once the rarefaction and the shock are separated, the behavior of the reconstruction scheme around the shock is driven by Theorem 2.5.

Test 3: Shock and shock

We consider the Riemann problem (1.3) with

$$\tau_L = 0.5,\ u_L = 2,\ \tau_R = 0.6 \quad \text{and} \quad u_R = 1.$$

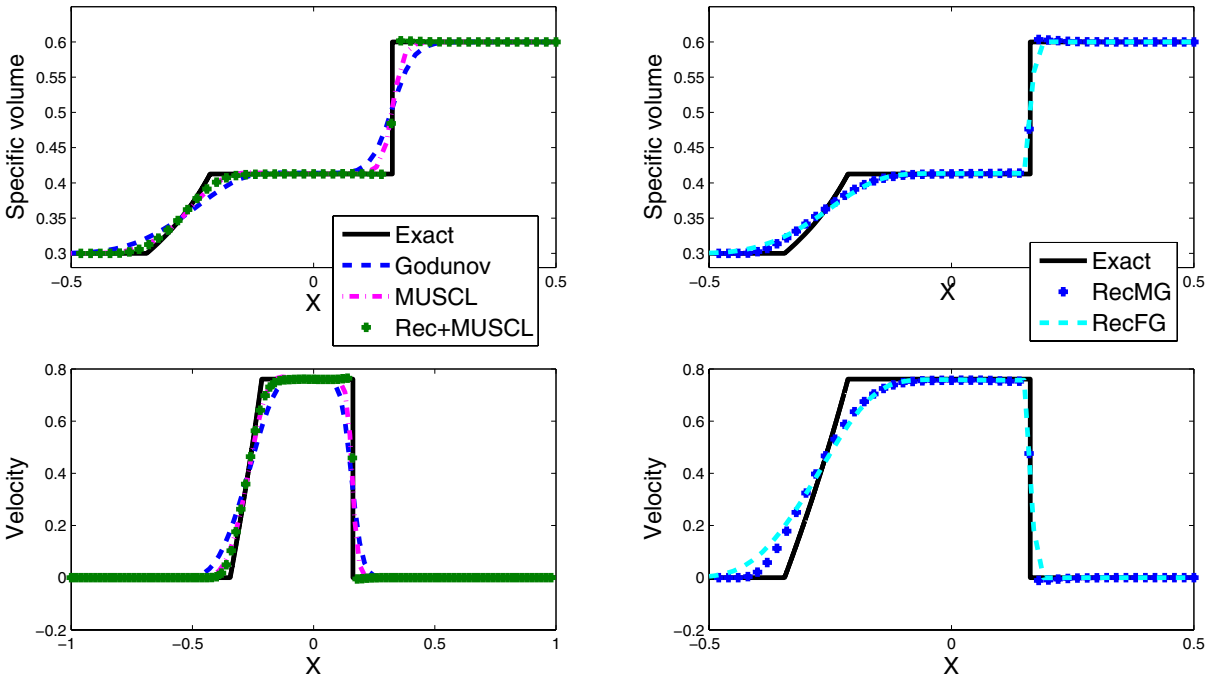

FIGURE 7. Test 2: Specific volume and velocity at time $t = 0.04$.

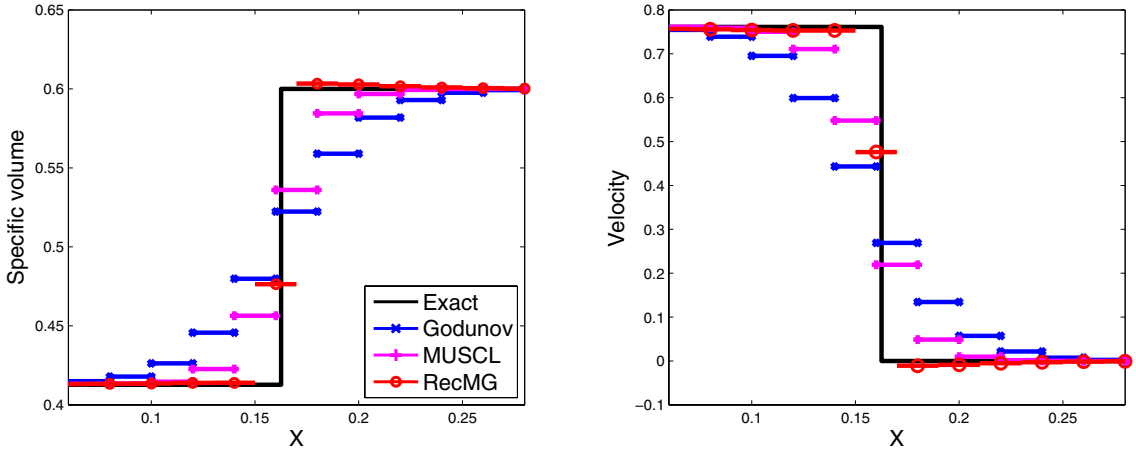

FIGURE 8. Test 2: Close-up on the piecewise constant shock profile.

It contains a 1-shock and a 2-shock. Figure 9 clearly demonstrates that they are both sharply captured, with only one point of numerical diffusion.

Test 4: Shock and strong shock

The aim of this test case is in some sense to test the robustness of Theorem 2.5. The initial Riemann data is given by (1.3) with

$$\tau_L = 1,\ u_L = 1,\ \tau_R = 52 \quad \text{and} \quad u_R = -8.$$

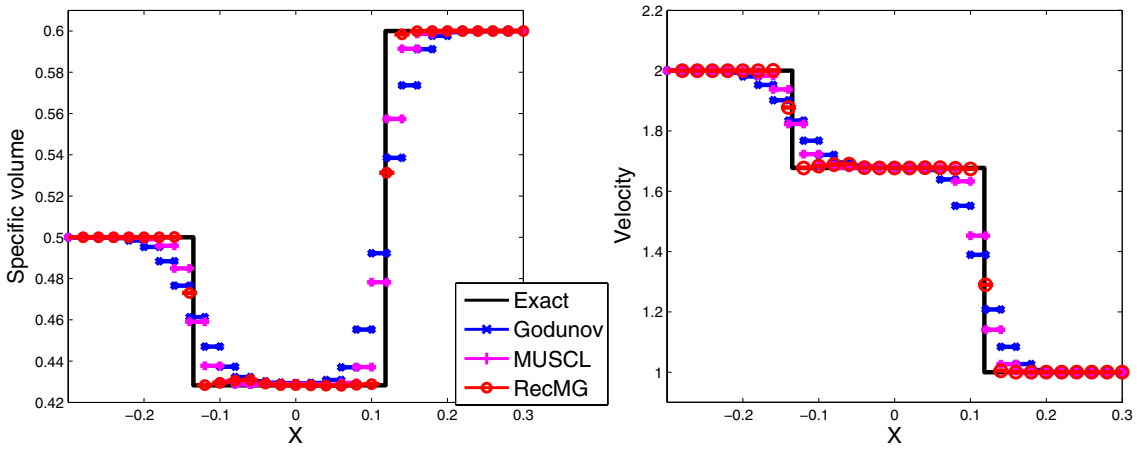

FIGURE 9. Test 3: Specific volume and velocity at time $t = 0.03$.

It is a slight modification of the fast shock considered in [4], in which the right state is $\tau_R = 50.981$ and $u_R = -6.068$, and the solution is an isolated 2-shock, and thus is covered by Theorem 2.5. With our modification, the solution also contains a nontrivial 1-wave of small strength.

When computing a strong shock (also called fast shock), spurious oscillations appear in the velocity when using usual Godunov-type methods. They also appear clearly in the characteristic variable $u \pm \sqrt{8/\tau}$. Those two quantities are plotted on Figure 10. Theorem 2.5 states that the scheme is exact on isolated strong shocks. We can see on Figure 10 that the ability of the reconstruction scheme to approach correctly fast shocks is not lost when we introduce a perturbation (here, a second wave in the Riemann problem).

Test 5: Isentropic compression

This test case consists in reversing the time starting from a developed 1-rarefaction wave, to recover a discontinuity. This is a difficult test case which shows a limitation of the discontinuous reconstruction strategy considered here, since we will see that the schemes do not satisfy the validity of a discrete entropy inequality (even though the computed solutions are perfectly admissible from a physical point of view).

Let us denote

$$(t,x) \mapsto U_{\rm rar}(x/t; U_L, U_R) = (\tau_{\rm rar}(x/t; U_L, U_R), u_{\rm rar}(x/t; U_L, U_R))$$

the self-similar rarefaction wave associated with the Riemann initial condition $U_L \mathbf{1}_{x<0} + U_R \mathbf{1}_{x\geq 0}$, with $U_L = (\tau_L, u_L)$, $U_R = (\tau_R, u_R)$ and

$$\tau_L = 0.5,\ u_L = 10,\ \tau_R = 5 \quad \text{and} \quad u_R = u_L - \sqrt{2}\left(\tau_R^{-1/2} - \tau_L^{-1/2}\right).$$

For this test case, the initial data is

$$\tau^0(x) = \tau_{rar}(-x/T_{\rm rar}) \quad u^0(x) = u_{rar}(-x/T_{\rm rar})$$

with $T_{\rm rar} = 0.2$. This initial condition is plotted on Figure 11. For times $t < T_{\rm rar}$, the exact solution is $U(t,x) = U_{rar}(-x/(T_{\rm rar} - t))$, and for times $t \geq T_{\rm rar}$, the solution coincides with the solution of the Riemann problem associated with *left* state U_R and *right* state U_L (at time $t - T_{\rm rar}$), which contains a 1-shock and a 2-rarefaction. In particular at time $t = T_{\rm rar}$ the exact solution is nothing but a discontinuity between U_R and U_L and located at $x = 0$.

We compare the reconstruction scheme on a moving grid and on a fixed grid at five different times. This is the only test case where the results are significantly different for the two schemes. On Figures 12–14 we plot the

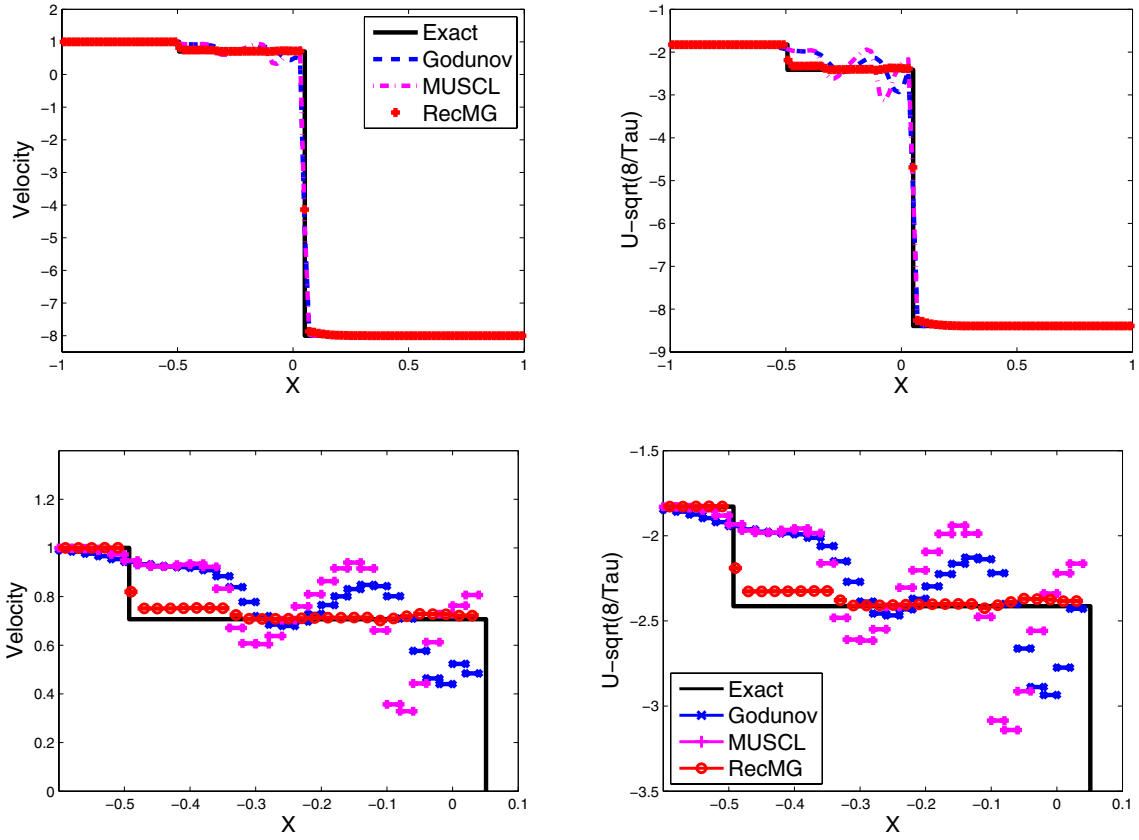

FIGURE 10. Test 4: Velocity (*left*) and $u - \sqrt{8/\tau}$ (*right*) at time $t = 0.3$. Domain $[-1 : 1]$ on the top and domain $[-0.6 : 0.1]$ on the bottom (close-up).

solutions for $t = 0.14$, $t = 0.17$, $t = 0.2$, $t = 0.23$ and $t = 0.26$. To ease the reading the x-axis is translated of 0.2 between two times; the dot indicates where $x = 0$ is. We observe a spike near the discontinuity when the time t is close to T_{rar}. It seems that the reconstruction scheme starts to reconstruct a little before $t = T_{\text{rar}}$ the expected shock that will appear in the exact solution for times $t > T_{\text{rar}}$, and that will be eventually sharply computed by the proposed schemes. The maximal height of the spike is at $t = T_{\text{rar}}$, and it diminishes rapidly afterwards, the shock being correctly approximated after T_{rar}. The spike does not prevent the scheme from converging in L^1, and its size is independent from the Courant number. On this test case, we observe that on the left of the solution, the results given on a fixed grid are much better than the ones given on a moving grid. On the other hand, we note that the Godunov-type scheme does not create any spike, but introduces numerical diffusion on the shock wave for times $t > T_{\text{rar}}$, as it is expected. On Figure 15, we plot the evolution of the entropy during the time interval $[0, 4]$ for this test case. More precisely, we plot the evolution of the quantity

$$\int \mathcal{U}(\tau^n_{\text{rec}}(x), u^n_{\text{rec}}(x))\mathrm{d}x - \int \mathcal{U}(\tau^{n-1}_{\text{rec}}(x), u^{n-1}_{\text{rec}}(x))\mathrm{d}x$$
$$+ (t^n - t^{n-1})((\mathcal{W}(\tau_R, u_R) - V^{n-1}_{\text{mesh}}\mathcal{U}(\tau_R, u_R)) - (\mathcal{W}(\tau_L, u_L) - V^{n-1}_{\text{mesh}}\mathcal{U}(\tau_L, u_L)))$$

where

$$\tau^n_{\text{rec}}(x) = \sum_j (\tau^n_{j,L}\mathbf{1}_{x<x^n_{j-1/2}+d^{n,\tau}_j} + \tau^n_{j,R}\mathbf{1}_{x\geq x^n_{j-1/2}+d^{n,\tau}_j})\mathbf{1}_{x\in\left[x^n_{j-1/2},x^n_{j+1/2}\right]}$$

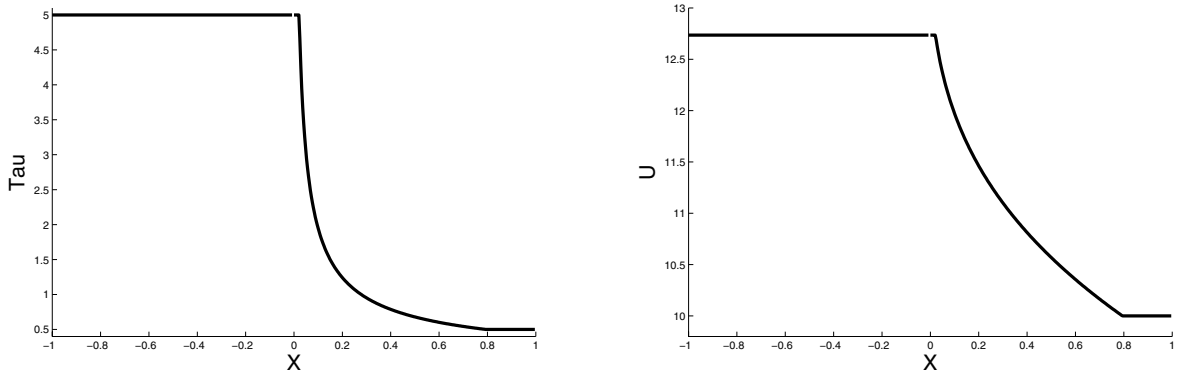

FIGURE 11. Initial condition for test 5.

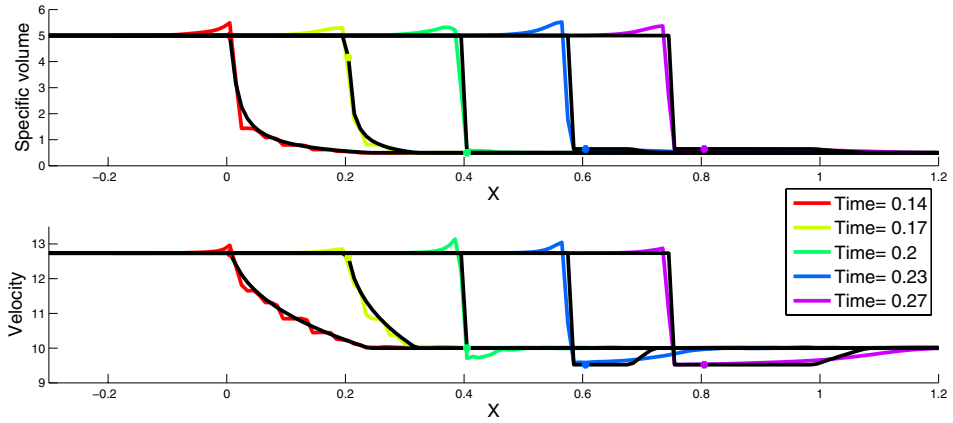

FIGURE 12. Solutions of test 5 at different times with the reconstruction scheme on a moving grid. The exact solutions are in black.

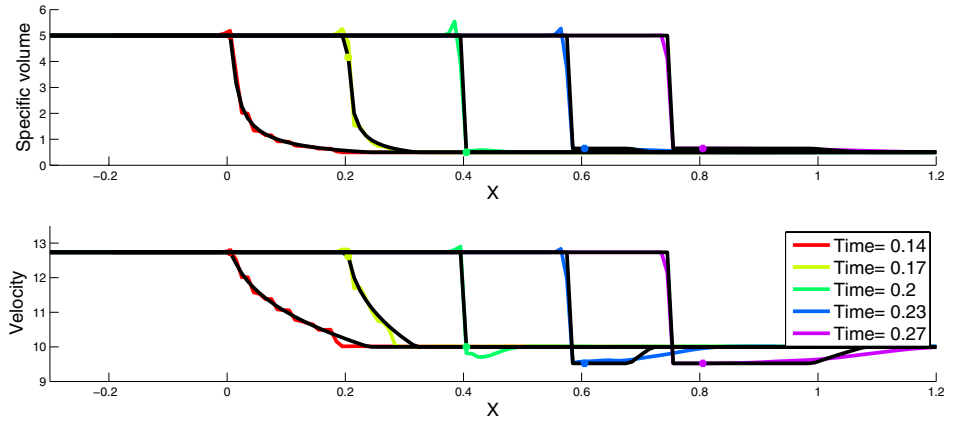

FIGURE 13. Solutions of test 5 at different times with the reconstruction scheme on a fixed grid. The exact solutions are in black.

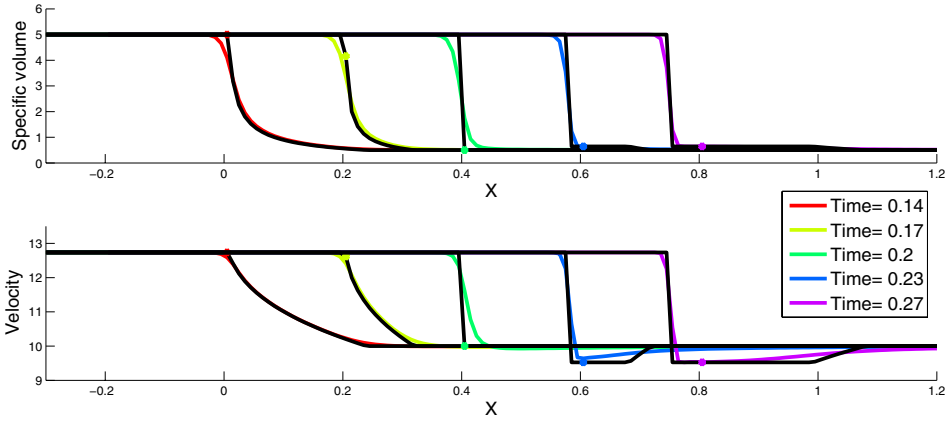

FIGURE 14. Solutions of test 5 at different times with the Godunov scheme. The exact solutions are in black.

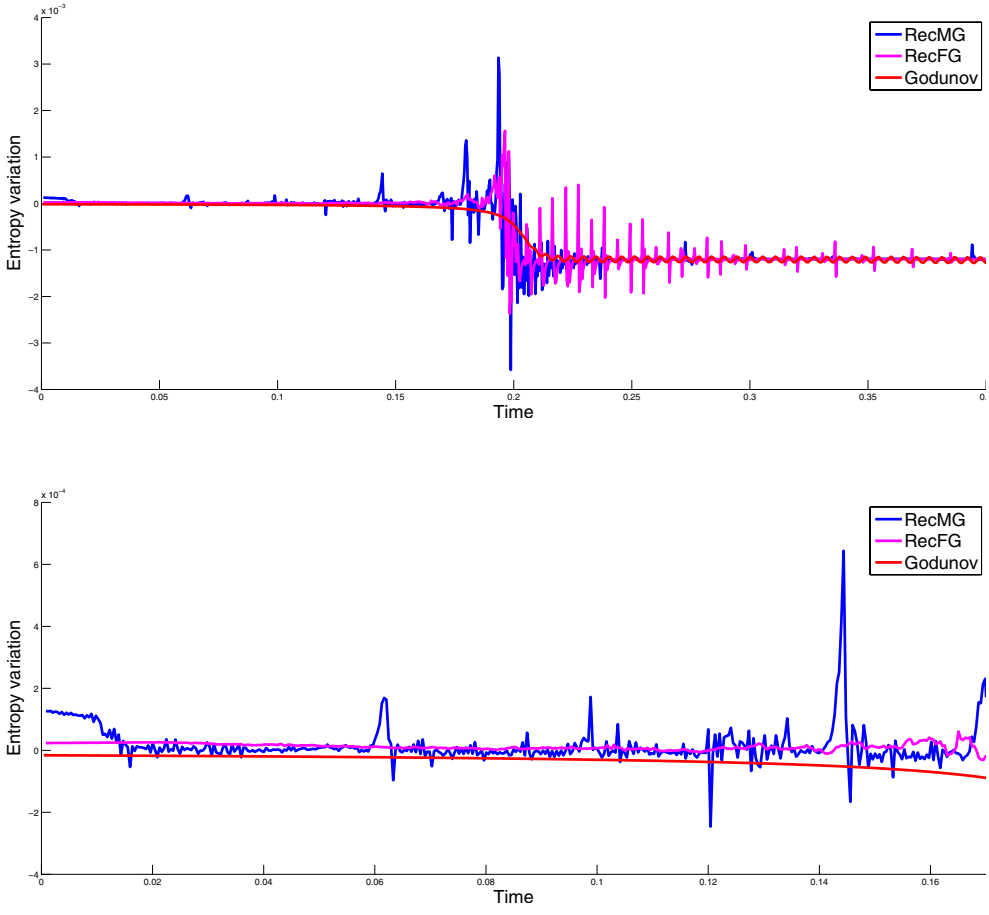

FIGURE 15. Evolution of the entropy through time in test 5, on the time interval $[0, 4]$ (*top*), and a zoom before time T_{rar} (*bottom*).

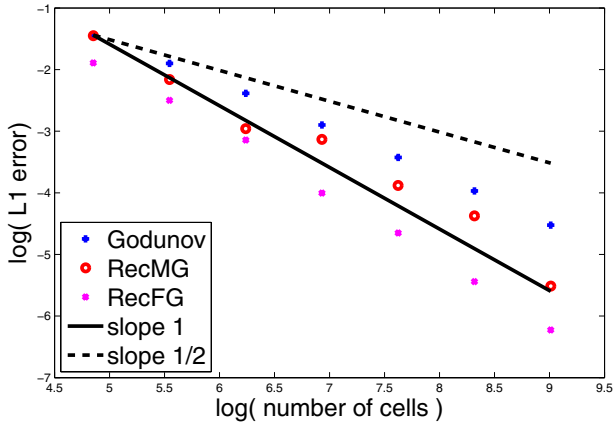

FIGURE 16. L^1-error at time T_{rar} with the Godunov-type scheme and with the discontinuous reconstruction schemes.

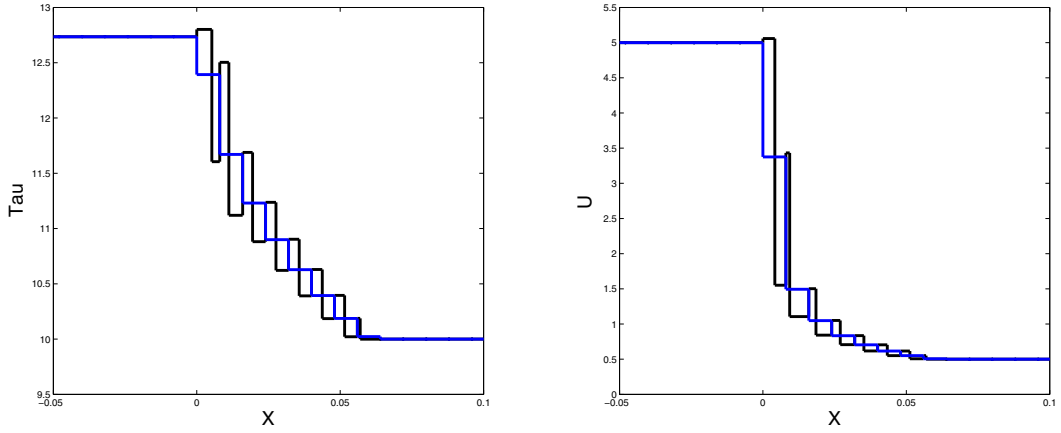

FIGURE 17. In black, the reconstructed solution U^0_{rec}, *i.e.* the solution reconstructed from the initial data before any iteration in time is done. We take $T_{\text{rar}} = 0.015$ and 500 cells. In blue, the piecewise constant function corresponding to $(U^0_j)_{j\in\mathbb{Z}}$. (Color online)

and

$$u^n_{\text{rec}}(x) = \sum_j (u^n_{j,L}\mathbf{1}_{x<x^n_{j-1/2}+d^{n,u}_j} + u^n_{j,R}\mathbf{1}_{x\geq x^n_{j-1/2}+d^{n,u}_j})\mathbf{1}_{x\in\left[x^n_{j-1/2},x^n_{j+1/2}\right]}$$

are the reconstructed solution at time t^n (we recall than on a fixed grid, $V^{n-1}_{\text{mesh}} = 0$ for all n). One can see that this quantity oscillates around 0 and often takes positive values until the time $T_{\text{rar}} = 0.2$. It indicates that the scheme is not entropy satisfying in the strict sense, but only in a "weak" sense to be defined. Indeed, the scheme seems to converge toward the correct solution in the L^1-norm. The order of convergence is plotted on Figure 16. Note also that even though the scheme is not entropy satisfying, it contains entropy information since the underlying approximate Riemann solver of [11] is entropy satisfying. It is thus likely that the problem comes from the discontinuous reconstruction strategy. More precisely, we believe that some reconstructions are not entropy satisfying and should be cancelled using a stronger constraint than the ones proposed in (2.17) and (2.18) (*i.e.* $d^{n,\tau}_j \in [0, \Delta x]$ and $d^{n,u}_j \in [0, \Delta x]$). For example in this case, we expect the reconstructed solution $U^n_{\text{rec}} = (\tau^n_{\text{rec}}, u^n_{\text{rec}})$ to be monotonous for times $t < T_{\text{rar}}$, but as depicted on Figure 17, this is not the case at all

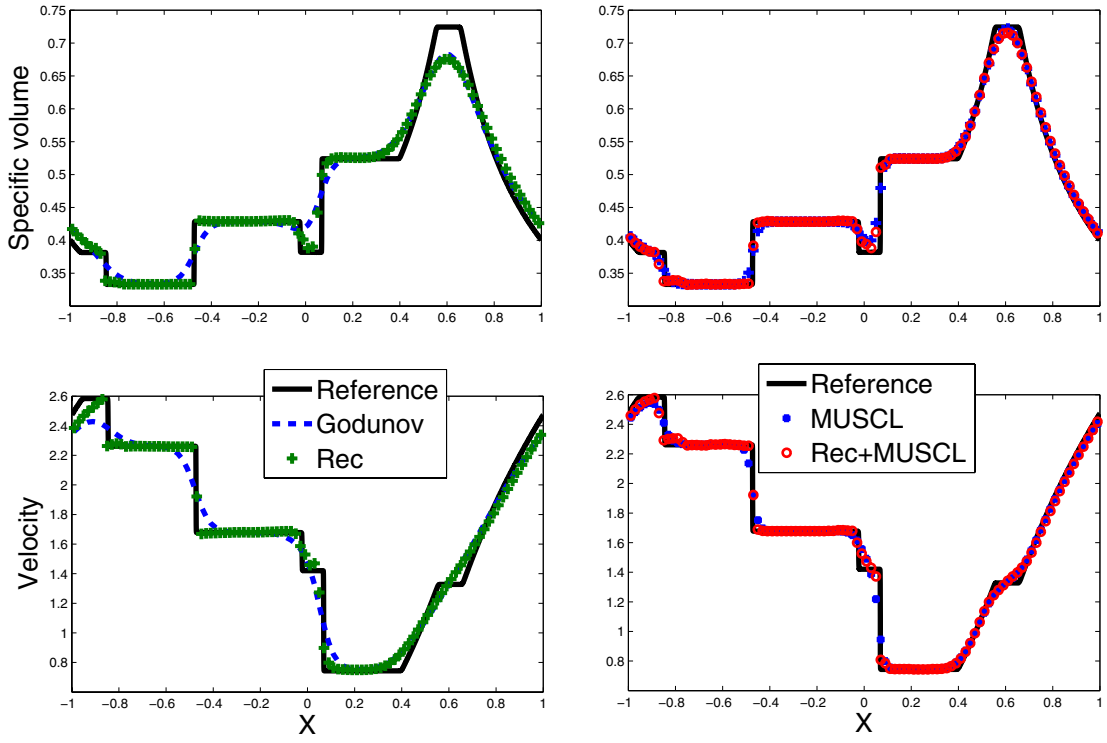

FIGURE 18. Test 6: Comparison at time 0.1.

in the course of the first iteration ($n = 0$). In the scalar case, entropy satisfying versions of the anti-diffusive scheme of [16] (which can be reinterpreted in terms of discontinuous reconstruction) have been proposed in [6], but remain to be adapted to the present setting. It is a challenging and open problem at the stage of the present work.

Test 6: Waves interactions

The aim of this test case is to test the ability of the reconstruction scheme to properly deal with waves interactions. We will consider both rarefaction/shock and shock/shock interactions at the same time. The initial data is

$$\begin{cases} \tau^0(x) = 0.5 * \mathbf{1}_{x\leq -1/3} + 0.6 * \mathbf{1}_{-1/3<x<1/3} + 0.3 * \mathbf{1}_{x\geq 1/3} \\ u^0(x) = 2 * \mathbf{1}_{x\leq -1/3} + \mathbf{1}_{-1/3<x<1/3} + 2 * \mathbf{1}_{x\geq 1/3} \end{cases}$$

on the interval $[-1, 1]$ with periodic boundary conditions. One thus have three distinct Riemann problems, each of them containing 2 distinct waves. We compare the reconstruction scheme (`Rec`) and the reconstruction scheme coupled with the MUSCL-Hancock strategy (`Rec+MH`), both on moving grids, with the Godunov scheme with and without MUSCL-Hancock strategy. The results are displayed on Figures 18–20 at times 0.1, 0.3 and 0.6. At these times, several waves interactions have already taken place. We observe that the shocks are still extremely sharp with the reconstruction schemes (only 1 or 2 intermediate values), even for long times.

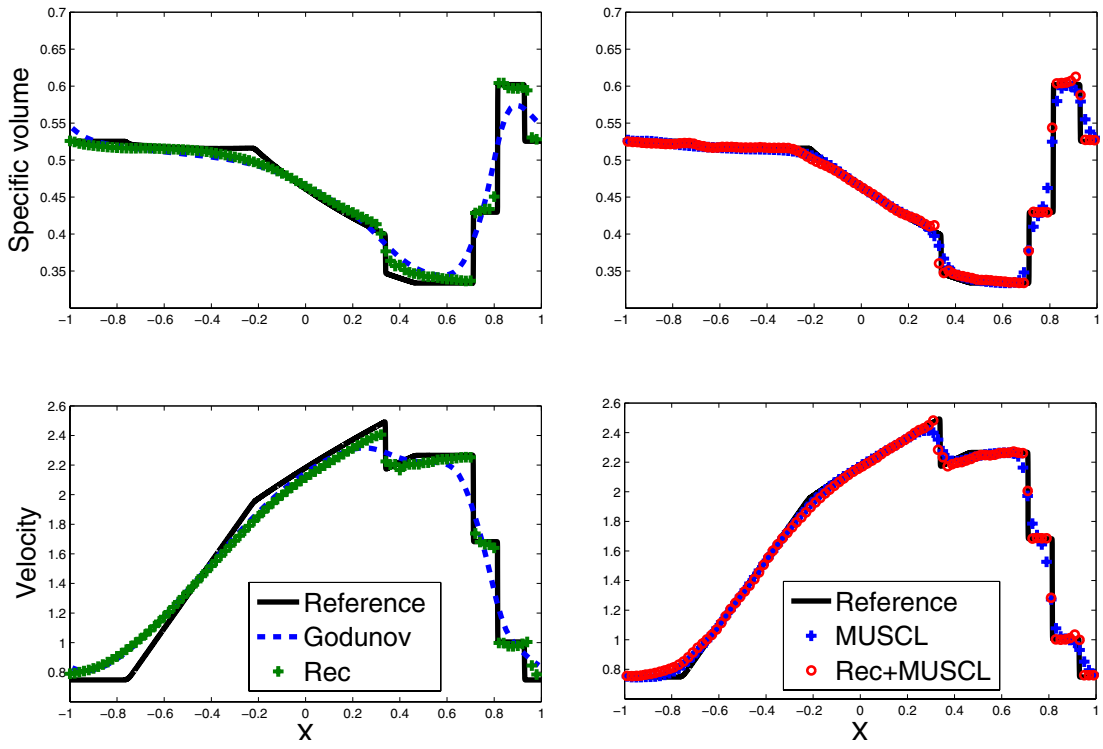

FIGURE 19. Test 6: Comparison at time 0.3.

4. Two dimensional simulations

In two space dimensions, the p-system writes

$$\begin{cases} \partial_t \tau - \partial_x u - \partial_y v = 0, \\ \partial_t u + \partial_x p(\tau) = 0, \\ \partial_t v + \partial_y p(\tau) = 0, \\ \tau(0,x,y) = \tau^0(x,y),\ u(0,x,y) = u^0(x,y),\ v(0,x,y) = v^0(x,y), \end{cases} \tag{4.1}$$

where u and v denote the horizontal and vertical velocity components. In order to extend the method proposed in the previous sections to 2D configurations, we propose to consider cartesian meshes and to use a standard directional splitting strategy. More precisely, the approximate solution $(\tilde\tau(\Delta t,x,y), \tilde u(\Delta t,x,y), \tilde v(\Delta t,x,y))$ of (4.1) at time Δt will be defined thanks to the following two steps. One first define $(\bar\tau(\Delta t,x,y), \bar u(\Delta t,x,y), \bar v(\Delta t,x,y))$ as the solution at time Δt of (4.1) in the x-direction, namely

$$\begin{cases} \partial_t \tau - \partial_x u = 0, \\ \partial_t u + \partial_x p(\tau) = 0, \\ \partial_t v = 0, \\ \tau(0,x,y) = \tau^0(x,y),\ u(0,x,y) = u^0(x,y),\ v(0,x,y) = v^0(x,y). \end{cases} \tag{4.2}$$

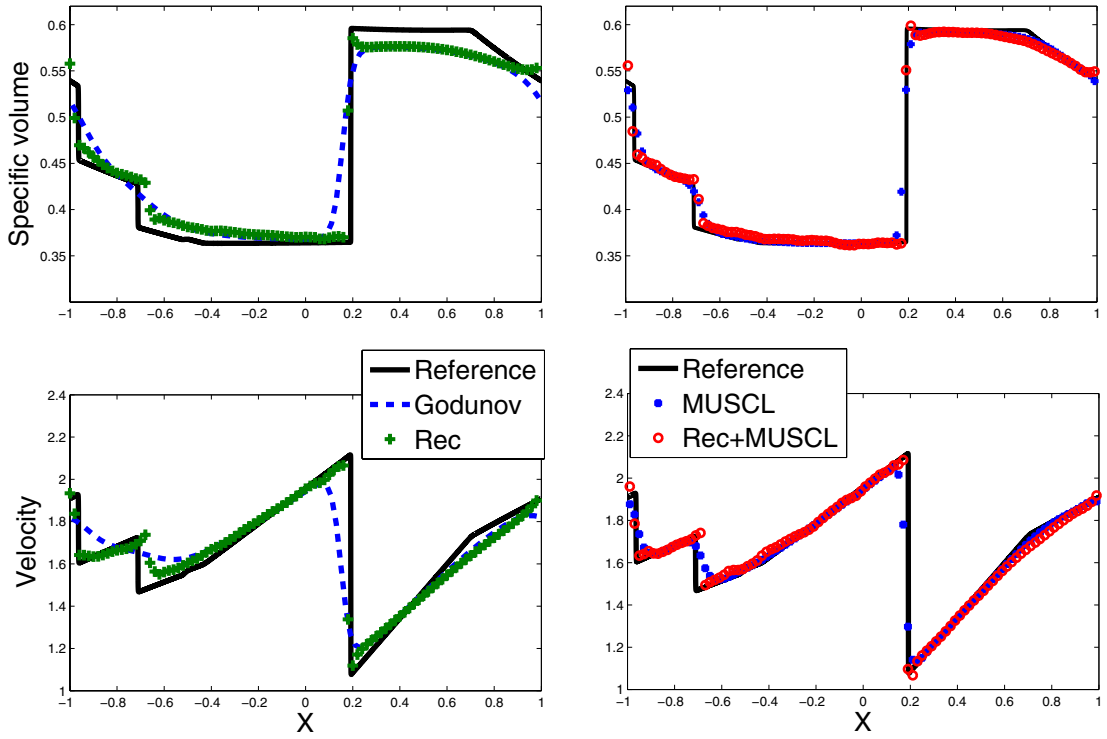

FIGURE 20. Test 6: Comparison at time 0.6.

Note that the initial condition in (4.2) is the same as in (4.1). In the second step, we define $(\tilde{\tau}(\Delta t, x, y), \tilde{u}(\Delta t, x, y), \tilde{v}(\Delta t, x, y))$ as the solution at time Δt of (4.1) but now in the y-direction, namely

$$\begin{cases} \partial_t \tau - \partial_y v = 0, \\ \partial_t u = 0, \\ \partial_t v + \partial_y p(\tau) = 0, \\ \tilde{\tau}(0, x, y) = \bar{\tau}(\Delta t, x, y), \ \tilde{u}(0, x, y) = \bar{u}(\Delta t, x, y), \ \tilde{v}(0, x, y) = \bar{v}(\Delta t, x, y), \end{cases} \tag{4.3}$$

where the initial condition is now taken to be equal to the solution obtained at the end of the first step. Using cartesian grids then allows to simply apply the $1D$ schemes proposed in the previous section to approximate the solutions of (4.2) and (4.3).

The numerical simulations are performed on a fixed grid with the pressure law $p(\tau) = \tau^{-2}$ and we compare as before the approximate solutions given by the reconstruction scheme (`Rec` in the legend), the reconstruction scheme coupled with a MUSCL-Hancock strategy (`RecMH`), the Godunov type scheme (`God`) and the MUSCL-Hancock scheme (`MH`).

4.1. Oblique shock and strong shock

We first start by reproducing the Test 4 of the $1D$ section in $2D$, considering that the direction of propagation of the shock is not aligned with the mesh and given by $(\cos(\theta), \sin(\theta))$. The initial data is

$$\begin{cases} \tau^0(x, y) = \mathbf{1}_{\cos(\theta)x + \sin(\theta)y \leq 0} + 52 * \mathbf{1}_{\cos(\theta)x + \sin(\theta)y > 0}, \\ u^0(x, y) = \cos(\theta) * \mathbf{1}_{\cos(\theta)x + \sin(\theta)y \leq 0} - 8\cos(\theta) * \mathbf{1}_{\cos(\theta)x + \sin(\theta)y > 0}, \\ v^0(x, y) = \sin(\theta) * \mathbf{1}_{\cos(\theta)x + \sin(\theta)y \leq 0} - 8\sin(\theta) * \mathbf{1}_{\cos(\theta)x + \sin(\theta)y > 0}, \end{cases}$$

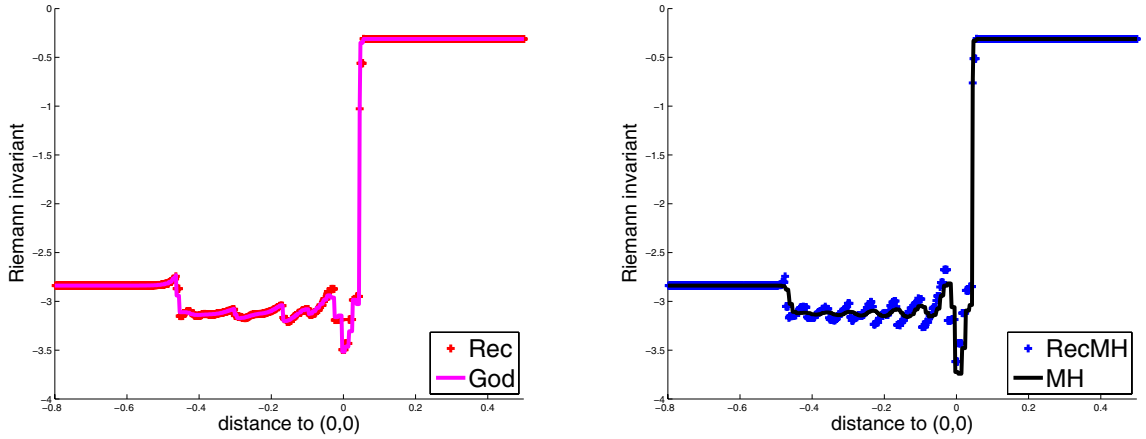

FIGURE 21. Apparition of oscillations in the Riemann invariant.

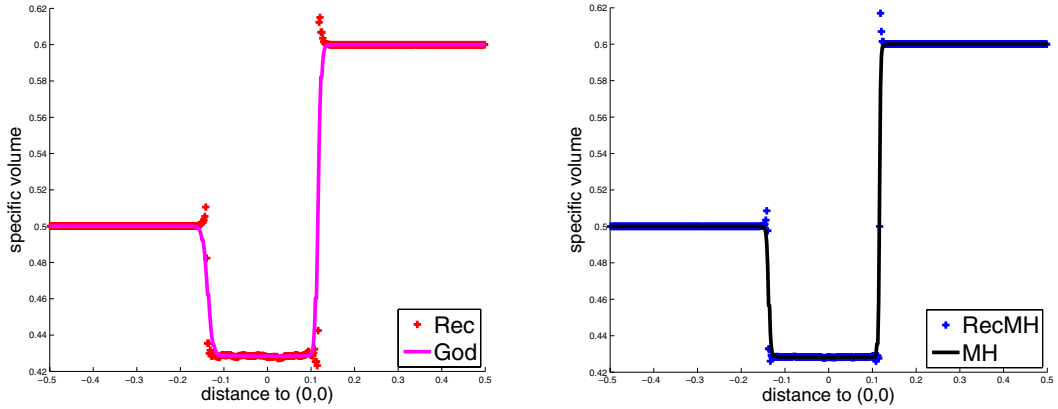

FIGURE 22. Comparison of several schemes on a oblique Riemann problem.

and we take $\theta = \frac{\pi}{4} + 0.01$. The computational domain is the (x, y)-rectangle $[-1.5, 1.5] \times [-1, 1]$ and the mesh is made of 420×280 cells. The courant number is set to 0.45 and we consider Neumann boundary conditions. Figure 21 shows a $1D$-cut along the direction of propagation of the shock of the Riemann invariant $u_{//} - \sqrt{8/\tau}$ ($u_{//}$ is the velocity in the direction of propagation of the shock), for which the oscillation are the most visible. We observe that the ability of the reconstruction scheme to compute an isolated admissible shock exactly is lost. This is clearly expected and due to the fact that an isolated admissible oblique shock cannot be admissible in the x-direction and in the y-direction with the same left and right constant states. Obtaining an analogue of Theorem 2.5 for $2D$ admissible isolated shocks (whatever the direction of propagation is) is out of reach with the proposed $2D$ extension of the method. On the contrary, it certainly necessitates the development of a relevant genuinely $2D$ extension of the $1D$ method (instead of using a directional splitting) together with new ideas.

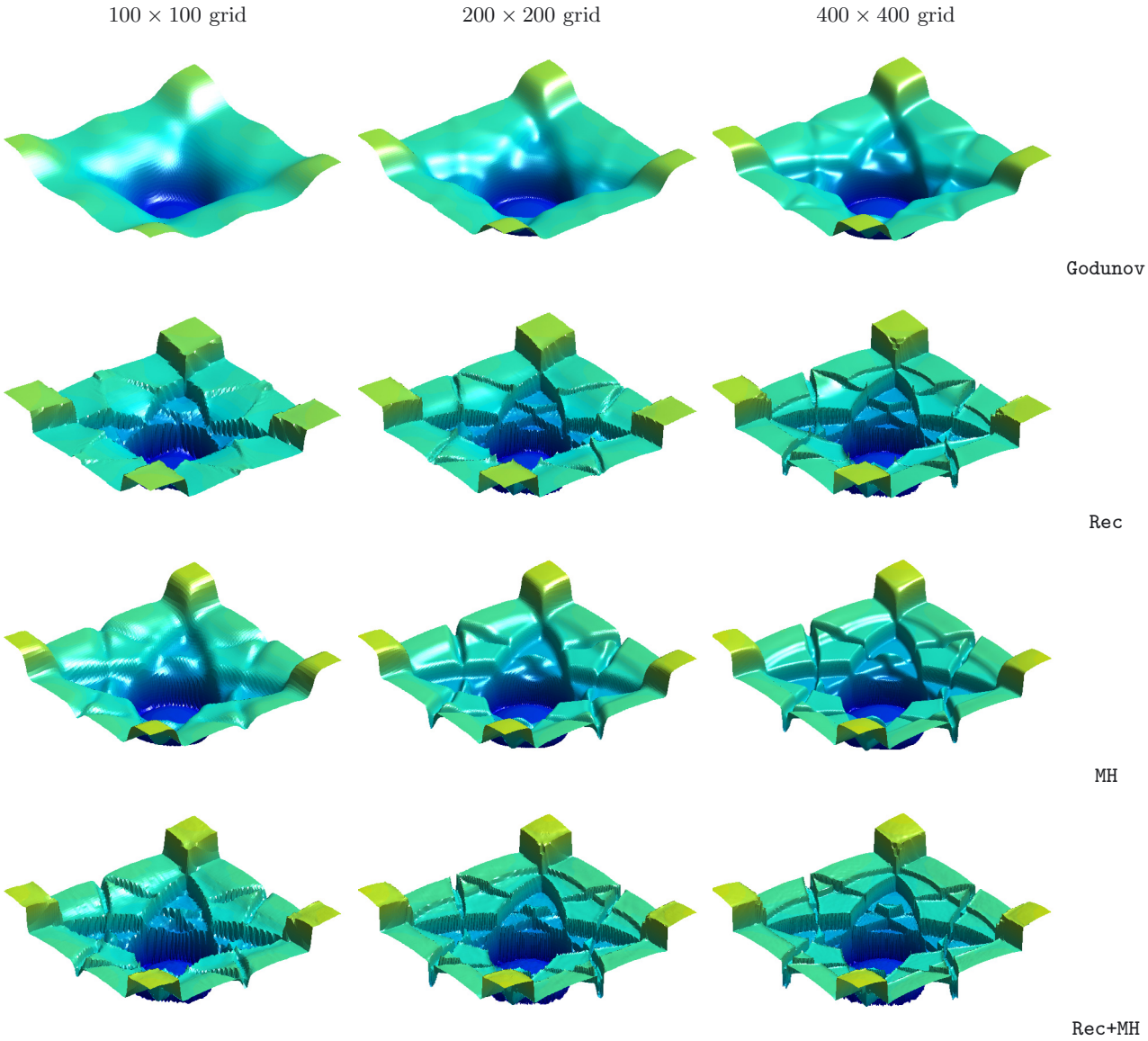

FIGURE 23. Solutions at time 4.5.

4.2. Oblique Riemann problem

This test case corresponds to the Test 3 of the $1D$ section but it is now performed in $2D$ with a direction of propagation given by $(\cos(\theta), \sin(\theta))$ with $\theta = \frac{\pi}{4} + 0.01$. More precisely, the initial data is given by

$$\begin{cases} \tau^0(x,y) = 0.5 * \mathbf{1}_{\cos(\theta)x+\sin(\theta)y\leq 0} + 0.6 * \mathbf{1}_{\cos(\theta)x+\sin(\theta)y>0}, \\ u^0(x,y) = 2 * \cos(\theta) * \mathbf{1}_{\cos(\theta)x+\sin(\theta)y\leq 0} + \cos(\theta) * \mathbf{1}_{\cos(\theta)x+\sin(\theta)y>0}, \\ v^0(x,y) = 2 * \sin(\theta) * \mathbf{1}_{\cos(\theta)x+\sin(\theta)y\leq 0} + \sin(\theta) * \mathbf{1}_{\cos(\theta)x+\sin(\theta)y>0}, \end{cases}$$

and the space and time discretizations are the same as in the previous $2D$ simulation. Figure 22 shows a $1D$-cut of the specific volume along the first diagonal. One can observe that the proposed reconstruction strategy

gives sharp shock profiles but at the price of significant overshoots and undershoots compared to the Godunov scheme. Unfortunately, we are not able to propose a precise explanation of such a behaviour. However, we believe that developing a reconstruction criterion which takes into account the validity of an entropy inequality might significantly improve the quality of the results.

4.3. 2D implosion

To conclude this section, we present a genuine $2D$ simulation. The computational domain is the square $[-1,1]^2$ with rigid wall boundary conditions, and the initial data is taken to be

$$\begin{cases} \tau^0(x,y) = \mathbf{1}_{\sqrt{x^2+y^2}\geq 0.5} + 2 * \mathbf{1}_{\sqrt{x^2+y^2}<0.5}, \\ u^0(x,y) = v^0(x,y) = 0, \end{cases}$$

which corresponds to a fluid at rest ($u = v = 0$) with a smaller density inside the circle which has its center at point $(0,0)$ and a radius of 0.5. We consider a Courant number of 0.45 and a fixed grid made of 100×100, 200×200 and 400×400 cells. Figure 23 shows that the specific volume is much less diffused with the reconstruction scheme than with the Godunov scheme. However, oscillations are still present with the reconstruction scheme.

5. Conclusions and perspectives

We proposed in this paper a new conservative finite volume method for the gas dynamics equations in Lagrangian coordinates. The method is based on the use of a relevant approximate Riemann solver which has the property of being exact for isolated admissible shock discontinuities, together with an in-cell discontinuous reconstruction strategy in order to remove the numerical diffusion near such discontinuities. Theorem 2.5 shows that the $1D$ scheme is exact for isolated shock waves, and numerical results prove that it captures discontinuities very sharply in more general situations. Despite the real quality of the numerical results, it was observed numerically that the numerical scheme may exhibit oscillations and not satisfy a discrete entropy inequality. The first main perspective of this work is thus to propose a stronger reconstruction criterion to ensure the validity of this property, which means in some sense adding numerical diffusion by removing the reconstruction step in the regions where the property is false, but without affecting the validity of Theorem 2.5. Entropy fixes for numerical schemes based on a reconstruction strategy have already been proposed in [21] for scalar conservation laws, but their extension to the system case is not trivial at all.

We performed $2D$ numerical simulations with the proposed method by simply considering cartesian meshes and a classical directional splitting strategy so that the $1D$ scheme could be used without any modification in each direction x and y. We obtained good and promising numerical results but the consequences of such a simple approach is that the validity of Theorem 2.5 is clearly lost, while the drawbacks related to the validity of an entropy inequality and the possible presence of oscillations are still present. To our opinion, the second main perspective of this work is to find a genuinely multidimensional extension of the $1D$ reconstruction scheme (instead of using a simple directional splitting) so that the validity of Theorem 2.5 is not lost. This issue is completely open at the moment.

At last, extending the proposed reconstruction scheme to the full system of gas dynamics (with energy equations) in Lagrangian and Eulerian coordinates is already a relevant perspective in $1D$.

Acknowledgements. This work was partially supported by a public grant as part of the Investissement d'avenir project, reference ANR-11-LABX-0056-LMH, LabEx LMH.

References

[1] N. Aguillon, Capturing nonclassical shocks in nonlinear elastodynamic with a conservative finite volume scheme. *Interfaces Free Bend.* **18** (2016) 137–159.

[2] N. Aguillon, A reconstruction scheme for the euler equations. Preprint `hal-00967484` (2016).

[3] F. Alouges, F. De Vuyst, G. Le Coq and E. Lorin, The reservoir technique: a way to make Godunov-type schemes zero or very low diffuse. Application to Colella-Glaz solver. *Eur. J. Mech. B Fluids* **27** (2008) 643–664.

[4] M. Arora and Ph.L. Roe, On postshock oscillations due to shock capturing schemes in unsteady flows. *J. Comput. Phys.* **130** (1997) 25–40.

[5] M.B. Friess, B. Boutin, F. Caetano, G. Faccanoni, S. Kokh, F. Lagoutière and L. Navoret, A second order anti-diffusive Lagrange-remap scheme for two-component flows. In *CEMRACS'10 research achievements: numerical modeling of fusion.* Vol. 32 of *ESAIM Proc.* **32** (2011) 149–162.

[6] F. Bouchut, An antidiffusive entropy scheme for monotone scalar conservation laws. *J. Sci. Comput.* **21** (2004) 1–30.

[7] F. Bouchut, A reduced stability condition for nonlinear relaxation to conservation laws. *J. Hyperbolic Differ. Equ.* **1** (2004) 149–170.

[8] F. Bouchut and T. Morales de Luna, Semi-discrete entropy satisfying approximate Riemann solvers. The case of the Suliciu relaxation approximation. *J. Sci. Comput.* **41** (2009) 483–509.

[9] B. Boutin, Ch. Chalons, F. Lagoutière and Ph.G. LeFloch, Convergent and conservative schemes for nonclassical solutions based on kinetic relations. I. *Interfaces Free Bound.* **10** (2008) 399–421.

[10] Ch. Chalons and F. Coquel, Navier-stokes equations with several independent pressure laws and explicit predictor-corrector schemes. *Numer. Math.* **101** (2005) 451–478.

[11] Ch. Chalons and F. Coquel, Modified Suliciu relaxation system and exact resolution of isolated shock waves. *Math. Models Methods Appl. Sci.* **24** (2014) 937–971.

[12] Ch. Chalons and J.-F. Coulombel, Relaxation approximation of the euler equations. *J. Math. Anal. Appl.* **348** (2008) 872–893.

[13] Ch. Chalons, M. Laura Delle Monache and P. Goatin, A conservative scheme for non-classical solutions to a strongly coupled pde-ode problem. Preprint `hal-01070262` (2014).

[14] G. Qiang Chen, C. David Levermore and Tai-Ping Liu, Hyperbolic conservation laws with stiff relaxation terms and entropy. *Comm. Pure Appl. Math.* **47** (1994) 787–830.

[15] F. Coquel, Shi Jin, Jian-Guo Liu and Li Wand, Entropic sub-cell shock capturing schemes via jin-xin relaxation and glimm front sampling for scalar hyperbolic conservation laws. Available at `http://www.math.wisc.edu/~jin/research.html` (2016).

[16] B. Després and F. Lagoutière, Contact discontinuity capturing schemes for linear advection and compressible gas dynamics. *J. Sci. Comput.* **16** 479–524 (2002), 2001.

[17] E. Godlewski and P.-A. Raviart, Numerical approximation of hyperbolic systems of conservation laws, Vol. 118 of *Appl. Math. Sci.* Springer-Verlag, New York (1996).

[18] S.K. Godunov, A difference method for numerical calculation of discontinuous solutions of the equations of hydrodynamics. *Mat. Sb. (N.S.)* **47** (1959) 271–306.

[19] A. Harten, ENO schemes with subcell resolution. *J. Comput. Phys.* **83** (1989) 148–184.

[20] Sh. Jin and Z.P. Xin, The relaxation schemes for systems of conservation laws in arbitrary space dimensions. *Comm. Pure Appl. Math.* **48** (1995) 235–276.

[21] F. Lagoutière, Non-dissipative entropy satisfying discontinuous reconstruction schemes for hyperbolic conservation laws. Available at `http://www.math.u-psud.fr/~lagoutie/Papiers/disc_reconst.pdf` (2016).

[22] F. Lagoutière, Stability of reconstruction schemes for scalar hyperbolic conservation laws. *Commun. Math. Sci.* **6** (2008) 57–70.

[23] H. Li, Zh. Wang and De-kang Mao, Numerically neither dissipative nor compressive scheme for linear advection equation and its application to the Euler system. *J. Sci. Comput.* **36** (2008) 285–331.

[24] H. Nessyahu and E. Tadmor, Nonoscillatory central differencing for hyperbolic conservation laws. *J. Comput. Phys.* **87** (1990) 408–463.

[25] I. Suliciu, On the thermodynamics of rate-type fluids and phase transitions. I. Rate-type fluids. *Internat. J. Engrg. Sci.* **36** (1998) 921–947.

[26] E.F. Toro. Riemann solvers and numerical methods for fluid dynamics. 3rd edition. Springer-Verlag, Berlin (2009). A practical introduction.

[27] B. van Leer, Towards the ultimate conservative difference scheme. V. A second-order sequel to Godunov's method. *J. Comput. Phys.* **135** (1997) 227–248.